

Transport of Ionizing Radiation in Terrestrial-like Exoplanet Atmospheres

David S. Smith¹, John Scalo, and J. Craig Wheeler²

Department of Astronomy, The University of Texas at Austin, Austin, TX 78712

ABSTRACT

The propagation of ionizing radiation through model atmospheres of terrestrial-like exoplanets is studied for a large range of column densities and incident photon energies using a Monte Carlo code we have developed to treat Compton scattering and photoabsorption. Incident spectra from parent star flares, supernovae, and gamma-ray bursts are modeled and compared to energetic particles in importance. Large irradiation events with fluences of 10^6 – 10^9 erg cm $^{-2}$ at the conventional habitable zone can occur at a rate from many per day (flares from young low-mass parent stars) to ~ 100 per Gyr (supernovae and gamma-ray bursts). We find that terrestrial-like exoplanets with atmospheres thinner than about 100 g cm $^{-2}$ block nearly all X-rays, but transmit and reprocess a significant fraction of incident γ -rays, producing a characteristic, flat surficial spectrum. Thick atmospheres ($\gtrsim 100$ g cm $^{-2}$) efficiently block even γ -rays, but nearly all the incident energy is redistributed into diffuse UV and visible aurora-like emission, increasing the effective atmospheric transmission by many orders of magnitude. Depending on the presence of molecular UV absorbers and atmospheric thickness, up to 10% of the incident energy can reach the surface as UV reemission. For the Earth, between 2×10^{-3} and 4×10^{-2} of the incident flux reaches the ground in the biologically effective 200–320 nm range, depending on O₂/O₃ shielding. For atmospheres thicker than ~ 50 g cm $^{-2}$ in the case of pure Rayleigh scattering and ~ 100 g cm $^{-2}$ in the case of O₂/O₃ absorption, the UV reemission exceeds the surficial transmitted ionizing radiation. We also discuss the effects of angle of incidence and derive a modified two-stream approximation solution for the UV transfer. Finally, we suggest that transient atmospheric ionization layers can be frequently created at altitudes lower than the equilibrium layers that result from steady irradiation and winds from the parent star. We suggest that these events can produce frequent fluctuations in atmospheric ionization levels and surficial UV fluxes on terrestrial-like planets.

Subject headings: Astrobiology; Radiative transfer: scattering; Photochemistry: Processes caused by X-rays or γ -rays; Extrasolar planets

¹Harrington Doctoral Fellow, NSF Graduate Research Fellow

²E-mail: {dss,parrot,wheel}@astro.as.utexas.edu

1. Introduction

Planets orbiting the Sun and other stars are occasionally subjected to large ionizing fluxes from astronomical sources, such as gamma-ray bursts, supernovae, and flares from the parent star. During these highly stochastic events, γ -ray, X-ray, and UV irradiation affects planetary atmospheric chemistry through ionization and heating, and biological activity through direct mutational enhancement or sterilization.

The frequency of the some types of these events has been estimated by Scalo and Wheeler (2002) and Scalo et al. (2003); see also §4. Rates and fluences for intense parent star flares are much more frequent for planets in the conventional habitable zone (continuous liquid water, see Kasting et al. 1993) of low mass stars; this is discussed briefly below in §4.1. Whatever the radiation source, the significance of the above phenomena depends strongly on the transparency of the atmosphere to the high-energy radiation. For this reason, we have studied the propagation of ionizing radiation (X-rays and γ -rays in our case) through a suite of model terrestrial-like exoplanet atmospheres of various column densities subjected to irradiation by various incident spectra. We also considered effects due to the angle of incidence.

Previous work has considered atmospheric irradiation by specific X-ray and γ -ray events (Brown 1973, Kasturirangan et al. 1976, Omongain and Baird 1976, Gehrels et al. 2003, and references therein), but only in a terrestrial context and, except for Gehrels et al. who studied the O_3 chemistry, were aimed at estimating only the altitude-dependent ionization. Some treated the radiative transfer in full detail while others used a simple exponential attenuation approximation. No past work has considered the electron excitation of atomic and molecular lines as a channel for redistribution of the ionizing flux to the biologically important ultraviolet spectral range, a major theme of the present paper. Our work also explores a large range of atmospheric column densities, follows the energy transfer in detail using a Monte Carlo approach, including accurate Compton and photoabsorption cross sections, and is generally concerned more with events that may affect planetary life. In particular, we are interested in events strong enough to result in biologically significant doses of radiation at the ground, as well as observable atmospheric chemical effects (e.g., photolysis, ionization, and heating).

In the present paper, we do not attempt to couple the radiative transfer to the atmospheric chemical or thermal structure; instead we assume an isothermal exponential atmosphere of given composition, column density, and scale height. This is an excellent approximation for the high-energy radiative transfer, in which the energies considered are much greater than typical molecular electronic binding energies, so the radiative transfer is basically independent of the chemical composition or thermal structure. We postpone a calculation of the impact on the chemical and thermal structure of the atmospheres, since our main focus is on the radiation that reaches the planetary surface. Specific application of the results of this work for Earth and Mars is given in Smith et al. (2004). Additionally, we are concerned with photon irradiation only. Energetic particles from the parent star or the Galaxy would induce similar processes and their energetics are briefly summarized

in §4.3.

Note that recent studies of irradiated “hot Jupiters” (e.g., Seager and Sasselov 1998) are concerned with the effect of the mostly visual radiation of the central star on giant planet atmospheres, not irradiation of terrestrial-like atmospheres by high-energy radiation. The present work has more in common with studies of irradiation of accretion disk atmospheres by compact high-energy radiation sources (Ross 1979; Kallman and McCray 1982; Ross and Fabian 1993). In addition, we confine our study to ionizing photons and neglect radiation produced through high-energy particle cascades (see Molina-Cuberos et al. 2001 and references therein for the case of Mars).

The kinds of events we are considering are of interest for their effects on the stability of planetary chemistry, but our primary motivation is the question of how and whether evolution would proceed on habitable planets immersed in a highly variable radiation environment. This question certainly includes the Earth, since it is likely that the terrestrial radiation environment has varied significantly over timescales from millennia to eons due to a variety of phenomena. Would an intermittently enhanced and stochastic radiation field and mutation rate inhibit or sterilize life, or instead accelerate its occurrence and evolution? In the simplest theoretical models for evolution at the level of allele frequencies, the rate of evolution is proportional to the variance of the allele probabilities, and this variance is increased by mutations. Thus one might reason that hypermutation events greatly widens the degree of variability on which selection can operate. The genetic response to hypermutation events or sudden environmental change, and the rate of evolution of the mutation rate itself, is complex (see for example Sniegowski et al. 2000). There is already some experimental evidence that evolutionary rates can be increased by enhanced rates of mutation (Itoh et al. 2002).

We are envisioning planetary biospheres in which environmental novelty and exogenous mutational variation is the norm. There are some tantalizing lines of evidence and arguments suggesting that diversity and hence evolution might be enhanced by an environment that is complex. Directed in vitro and artificial life evolution experiments both indicate that genome lengths (one metric of complexity) grow only in information-rich environments (see Adami et al. 2000). That the rate of evolution increases with environmental diversity or novelty has been demonstrated in organisms as simple as the yeast *Pseudomonas fluorescens* (Rainey and Travisano 1998) and as complex as guppies (Reznick et al. 1997). See also Moxon et al. (1994); Peak et al. (1996); van Belkum et al. (1998); Pinaud et al. (2002); Chesson and Huntly (1997). The recognition of the existence of hypermutability mediated by heat shock proteins (see Rutherford and Lindquist 1998; Feder and Hofmann 1999, and the overview by Pugliucci 2002) and mutator mutases (e.g., Giraud et al. 2001; Radman et al. 1999, 2000) are of particular relevance to the present work. Another line of evidence comes from considering evolution as a learning process. Experiments using neural networks as the phenotype for digital genomes show that learning is more efficient in the presence of bursts of strong mutation compared to a constant mutation rate (Moriarty and Miikkulainen 1995, 1999; Gomez and Miikkulainen 1997). From one perspective, mutations that increase fitness can be regarded as random measurements on the environment, and genomes as selection-imprinted genetic memory of

past environments (Adami et al. 2000). Flares, supernovae, and other stochastic radiation events may provide a wide information channel on which natural selection can operate.

This point of view should be contrasted with the assumption of Ward and Brownlee (2000) and Gonzalez et al. (2001) that development of complex organisms primarily requires self-regulated stability of the environment. Surely stability at some level (especially with respect to temperature) is desirable for the continuance and evolution of life, but between the extreme limits of tolerance, it is possible that development of complexity is enhanced by fluctuations, as the above examples suggest. If so, accelerated evolution and development of complexity may occur on habitable planets subjected to a strongly fluctuating radiation environment. This possibility is obviously of crucial importance for selection of targets in SETI searches (Turnbull and Tarter 2003). While we cannot yet demonstrate whether this occurs, or whether such an environment simply retards evolution or sterilizes life, the arguments given above suggest that an acceleration of evolution is plausible, and in any case motivates us to quantify the nature of the fluctuations themselves, in particular how well atmospheres of various column densities on terrestrial-like exoplanets are buffered from jolts of ionizing radiation.

2. Methods

2.1. Input

2.1.1. Exoplanet atmosphere model

Our work assumes an isothermal, plane-parallel atmosphere having an exponential vertical density distribution. Because of the high energies of the photons compared to the molecular thermal energies in the atmosphere, the value of the temperature is irrelevant for our calculations except insofar as it affects the scale height. Similarly, the photon energies are so large compared to electronic binding energies of atoms or molecules that the radiative transfer and secondary electron energy budget is approximately independent of the composition of the atmosphere; in effect the photons only “see” free electrons at these energies. The particular density values at each grid point are determined by specifying the total column density in g cm^{-2} , which determines the number density of particles at the ground n_0 . Using n_0 and h , we build up the grid according to $n_i = n_0 \exp(-z_i/h)$, where z_i is the altitude of the i -th grid point.

Choosing the scale height is fairly straightforward when using an exponential density distribution. In all quantities related to the radiative transfer, the scale height only appears in the product n_0h and the quotient z/h . The total column density of the atmosphere is n_0h , so fixing the column density (and hence the optical depth) and adjusting the scale height only changes the number density of molecules at the ground, which is irrelevant for our work. The one effect of choosing a particular scale height is that it sets the altitude scale in terms of z/h , i.e., the altitudes corresponding to given optical depths from the top of the atmosphere are determined by h . In this

work, we use the terrestrial scale height value of 8 km. The altitudes in our results for any other desired scale height may be determined according to

$$z' = \left(\frac{h}{8 \text{ km}} \right) z, \quad (1)$$

where z is the altitude given by our results, and z' is the altitude on the exoplanet with a scale height h .

If the habitability of an exoplanet is adequately defined by the presence of liquid water, the lower limit to the column density of a planet with surface liquid water is given by considerations of water vapor photodissociation followed by atmospheric escape (Ingersoll 1969; Kasting 1988; Kasting et al. 1993). An estimate of the lower limit is $30\text{--}100 \text{ g cm}^{-2}$ for a terrestrial mass planet, depending on the temperature (J. Kasting, private communication). This is also coincident with the smallest column density required to prevent atmospheric collapse on synchronously rotating planets ($\gtrsim 30 \text{ g cm}^{-2}$, as given by Joshi et al. 1997).

Avoiding speculation about the origins or robustness of life, for illustrative purposes we assume that planets possessing even thin atmospheres are indeed habitable—given enough warming flux from the parent star.

Selecting atmospheric constituents for terrestrial-like exoplanets is extremely speculative. Fortunately, we can neglect atmospheric composition effects on the radiative transfer of the incident ionizing radiation because the energies considered here are so much larger than any internal atomic or molecular transition energies of interest. The composition matters only in that it determines the column abundances of electrons, which are the primary scatterers. For simplicity, we chose an inert N_2 atmosphere for the transfer of ionizing radiation. None of the results for the ionizing radiation would change significantly if the primary constituent were CO_2 or O_2 .

The transfer of the UV reemission *does* depend on assumed composition are discussed (see §2.3). For this calculation, we chose two simple UV opacity sources that probably bracket the extremes of UV transparency. For present-day Earth analogues, we included O_2 and O_3 absorption, distributed in an abundance profile similar to Earth's (taken from Appendix C of Brasseur et al. 1999 for altitudes up to 60 km and from Table 14-7 of Champion et al. 1985 for larger altitudes). For column densities other than Earth's, we scaled the terrestrial O_3 altitude profile to match the vertical O_3 column density from the top of the exoplanet atmosphere, i.e., the peak of the O_3 profile is always at the same column density from the top. This could be a severe approximation—see §2.3.4. For Archean Earth analogues, we removed molecular absorption and included only Rayleigh scattering, although we recognize the possibility of other Archean UV screens (e.g., Sagan and Chyba 1997), especially aerosols. These two idealizations are useful to gauge the surficial UV fluence in different limits.

2.1.2. Incident radiation spectra

Given that we are interested in such sources as supernovae, gamma-ray bursts, and stellar flares, we chose incident spectra characteristic of these. For supernovae we assumed monoenergetic spectra of energies 0.125, 0.25, 0.5, 1, and 2 MeV (1 MeV = 1.24×10^{-3} nm), which correspond to the energy ranges of ^{56}Co and ^{56}Ni decay lines (Höflich et al. 1998). We chose not to model specific supernovae spectra—they are merely the motivation for using a monoenergetic spectrum, which is instructive in its simplicity. In order to model the effects of stellar flares and gamma-ray bursts, we included two types of continuous spectra.

To represent the lower-energy spectra of flares, we adopted the following parameterized formula which is actually the energy dependence expected for a high-temperature thermal plasma, such as the solar corona (Tucker and Koren 1971):

$$\frac{dN}{d\lambda} \propto \lambda^{-2} \exp(-\lambda_p/\lambda), \quad (2)$$

where $dN/d\lambda$ is the number of photons per unit wavelength. Our adopted spectral form for flares is also consistent with the 0.9–10 keV spectrum of the giant X-ray flare in the dMe star EV Lac presented by Favata et al. (2000). We are unaware of the expected or observed form of generic solar or stellar flare spectra; the problem is complicated by the fact that flares peak in different wavelength regimes at different times. For the energy spectrum corresponding to Eq. 2, the photon number distribution can be shown to be

$$\frac{dN}{dE} = \frac{N_\gamma}{E_p} \exp\left(-\frac{E}{E_p}\right), \quad (3)$$

where N_γ is the total number of photons in the model and $E_p = hc/\lambda_p$ is the energy corresponding to the peak of the wavelength spectrum (Eq. 2). We calculated models irradiated by flare spectra with peak energies, E_p , of 2.2, 22, and 220 keV, corresponding to average energies of 1, 10, and 100 keV (see Krucker and Lin 2002). For these spectra, the lower and upper photon energy cutoffs are $0.01E_{\text{inc}}$ and $4E_{\text{inc}}$, respectively, where E_{inc} is the specified average incident energy, from which the peak energy, E_p , was calculated. We chose to place the above arbitrary limits on the flare spectra for computational reasons: photons of higher energy than about $4E_{\text{inc}}$ are too improbable, and photons of energy much lower than $0.01E_{\text{inc}}$ are of little physical significance because of the low energies.

For the gamma-ray burst spectra, we used a broken power law with an exponential cutoff known as a Band spectrum (Band et al. 1993). The photon number distribution is given by

$$\frac{dN}{dE} = k \left(\frac{E}{100 \text{ keV}} \right)^\alpha \exp(-E/E_0) \quad (4)$$

for $E \leq (\alpha - \beta)E_0$ and

$$\frac{dN}{dE} = k \left[\frac{(\alpha - \beta)E_0}{100 \text{ keV}} \right]^{\alpha-\beta} e^{\beta-\alpha} \left(\frac{E}{100 \text{ keV}} \right)^\beta \quad (5)$$

for $E \geq (\alpha - \beta)E_0$, where $E_0 = 250$ keV is the turnover energy, α and β are the power law indices. We adopt for this particular spectrum upper and lower wavelength limits of 50 keV and 3 MeV, respectively, with an average energy of 200 keV (constrained by observations, e.g., Preece et al. 2000). The empirical power law indices lie in the range $-1.6 \lesssim \alpha \lesssim 0.0$ and $-4.5 \lesssim \beta \lesssim -1.5$ (Tavani et al. 2000). For our calculations, we adopt $\alpha = -0.9$ and $\beta = -2.3$, which are roughly the averages in the histograms given by Tavani et al.

We examined Band spectra, but for simplicity our results are given only for the model flare spectra and monoenergetic spectra. Since both the model flare spectra and Band spectra decline in photon number at higher energies, the results are very similar if the average energies are equal. Indeed, some of our results will be shown to be completely independent of the form of the incident spectrum. Additionally, gamma-ray bursts are such infrequent events that their contribution to the mutational environment of an exoplanet is much smaller than supernovae and stellar flares.

The angle of incidence was taken to be normal to the atmospheric boundary surface for most of the calculations. Given a point source in the sky, the angle of incidence will be roughly perpendicular for most of the planet. But the spherical symmetry of the problem still makes a calculation for normal incidence slightly more optimistic than one that included the full radiative transfer effects of varying the angle of incidence. We tested varying the angle of incidence and its effects on the transmitted fraction and discuss the results briefly in §3.4.2 below.

2.2. Incident ionizing radiation transfer

The transfer of the incident X-rays and γ -rays was handled via a Monte Carlo code that was written for this work and that accurately accounts for the complicated angular and energy dependences of the cross sections. Appendix B explains the algorithm in detail.

The initial step of the calculation involves Compton scattering and photoabsorption of γ -rays and X-rays. Compton scattering was implemented as an inelastic scattering cross section given by the Klein-Nishina formula (Lingenfelter and Rothschild 2000). Photoabsorption was included as a purely absorptive cross section of the empirical form

$$\sigma_{\text{pa}}(E, Z) = 2.04 \times 10^{-30} (1 + 0.008Z) \frac{Z^3}{E^3} \text{ cm}^2, \quad (6)$$

where Z is the atomic number of the absorber and E is the photon energy in units of the electron rest mass (Setlow and Pollard 1962). We found that Eq. 6 reasonably represented the detailed cross section measurements (Henke et al. 1993) for a variety of elements for energies greater than the corresponding K photoabsorption edge (480 eV for nitrogen).

Since terrestrial-like exoplanet atmospheres can be very optically thick to high-energy radiation (e.g., the optical depth is 65 at 1 MeV on the Earth), two weighting procedures were used to more efficiently track photon statistics (see Watson and Henney 2001 for a summary of weighting and

other variance reduction techniques). In our model, approximately 10^6 photons are initialized at the top of the atmosphere heading downward with energies sampled according to the specified incident spectrum. Supernovae and flare spectra were sampled by inversion, while the Band spectrum was sampled by a rejection technique (Hammersley and Handscomb 1979; Kalos and Whitlock 1986). Every photon carries a statistical weight, which signifies the probability that it is still scattering in the atmosphere after each interaction. Each photon is propagated to a random optical depth, sampled from $e^{-\tau}$, since the probability that the photon will travel a distance corresponding to τ without interaction is $e^{-\tau}$. The photon is then statistically forced to scatter by subtracting a fraction of its weight equal to the probability, $e^{-\tau}$, that it did not scatter before exiting the grid. This technique is known as “forced scattering” (Witt 1977). In this way, the statistics are more accurately tracked for a discrete number of photons, and each Monte Carlo interaction explores many possible outcomes. Mersenne Twister (Matsumoto and Nishimura 1998) was used for pseudo-random number generation.

During the above process, we tracked the spectra of photon energy deposited at the ground, electron energy deposited (via Compton recoil and photoabsorption) at various layers in the atmosphere, and photons lost to space. Later this information is used to calculate the UV reemission fluxes and ionization fractions.

2.3. UV redistribution

2.3.1. Physical process

The Earth receives a steady flux of solar wind ions with very high kinetic energies. Energetic electrons produced via a variety of mechanisms (fast particles, magnetohydrodynamic flows, etc.) excite atmospheric constituents, resulting in dynamic auroral displays that extend from the ultraviolet to the infrared. Chamberlain (1961) discusses the detailed physical mechanisms.

When astrophysical bursts of radiation, such as stellar flares, supernovae, and gamma-ray bursts irradiate a terrestrial-like exoplanet with a sufficiently thick atmosphere, analogous phenomena will occur. The initial ionizing radiation creates primary electrons as a photoproduct. These very energetic charged particles then produce secondary photoelectrons which excite molecules and create aurora-like emission in much the same way the solar wind and EUV does on Earth.

Since the energies considered here are so high, an incident photon can cause the ionization of tens of thousands of molecules before being absorbed. Primary Compton-recoil electrons and photoelectrons are responsible for the ionization as they are slowed by collisions with neutral N_2 molecules. Each of these ionizations results in a secondary electron, and it is these liberated electrons which dominate the particle flux from the incident radiation (see Evans 1974 for direct observations of auroral electron spectra). The average energy of secondary electrons released by primary ionization of N_2 is about 35 eV (Fano 1963), with only a very weak dependence on primary

electron energy or charge of the target. For example the average energy per ion pair for air, argon, and water are 34, 26, and 30 eV, respectively (see, for example, Fano 1963). The distribution of secondary energies has been studied experimentally by Peterson et al. (1971, 1972).

As each secondary electron moves through the atmosphere, it can exchange energy with other particles by (i) elastic Coulomb interactions and elastic collisions with neutrals (both of which lead to thermalization of the electron energy) or (ii) excitation of internal degrees of freedom in the target molecules. In case (ii), secondary electron impact excitation of electronic, vibrational, and rotational levels will result in a rich line spectrum extending from the UV (electronic transitions) to the radio (pure rotational transitions). This excitation by secondary electrons and subsequent line emission is equivalent to the main process giving rise to the terrestrial auroral spectra. In our case the process redistributes some of the energy of the X-ray and γ -ray photons into UV and longer wavelengths. This redistribution is also analogous to that which occurs in gases of cosmic abundances in accretion disks around compact stellar remnants (Ross 1979; Kallman and McCray 1982; Ross and Fabian 1993) and in interstellar clouds where secondaries from cosmic-ray ionization events can result in a rich UV line spectrum (Prasad and Tarafdar 1983; Gredel et al. 1989). An important difference between the molecular and atomic cases is that in the atomic case the secondary electron energy must be thermalized once its energy falls below the excitation potential of the first excited state of the atom, whereas the molecular case has a broad spectrum of excitation channels at lower energies.

2.3.2. *Excitation dominates heating*

In a highly ionized plasma, most of the electron energy would be thermalized by electron-electron collisions because of the long-range nature of the Coulomb interaction—very little of the energy would go into excitation and line radiation. The importance of electron-electron collisions depends on the ionization fraction, however, and for a nearly neutral planetary atmosphere, most of the secondary electron energy goes into excitation, not heating. Fox and Victor (1988) presented detailed calculations of the dependence on the ionization fraction of the number of excitations to various electronic levels of N_2 .

We can derive an order of magnitude condition for excitation to be more important than Coulomb interactions by comparing the respective collision frequencies. The characteristic Coulomb collision frequency can be expressed as (Spitzer 1978, Eqs. 4.13 and 4.14)

$$\nu_{ee} = \frac{4\pi e^4 n_e}{m_e^2 w^3} \ln \left(\frac{\Lambda m_e w^2}{3kT} \right), \quad (7)$$

where w is the relative velocity between test and field electrons and the factor

$$\Lambda \equiv \left(\frac{9k^3 T^3}{4\pi n_e e^6} \right)^{1/2} \quad (8)$$

is the usual approximate cutoff factor in the Coulomb logarithm—see Spitzer (1962) and Mitchner and Kruger (1973) for derivations. The extra ratio of energies in the logarithm accounts for the fact that the test particles follow a non-Maxwellian velocity distribution. Noting the $w^{-3} \propto E^{-3/2}$ dependence, we see that this agrees very well with the analytical fit to more detailed calculations given by Swartz et al. (1971):

$$\nu_{ee} = 2.0 \times 10^{-4} n_e^{0.94} E^{-1.44} \text{ sec}^{-1}, \quad (9)$$

where E is the energy of the secondary electrons in eV and $E \gg kT$. We adopt this convenient fit here. We neglect electron-ion Coulomb scattering because the time scale for thermalization by electron-ion scattering is larger than for electron-electron scattering because the high electron-ion mass ratio reduces the per-collision energy transfer efficiency.

We estimate the inelastic collision frequency to be

$$\nu_{inel} = n \sigma_{inel} (2E/m_e)^{1/2}. \quad (10)$$

The cross sections for ionization and excitation of N_2 and other atmospheric gases are energy dependent, with much structure due to resonances with dominant electronic and vibrational transitions as the secondary electron energy decreases. A useful plot of cross sections for N_2 , O_2 , and O from 1 to 100 eV is given in Banks and Kockarts (1973), and cross sections for N_2 at low energies are given in Fig. II.43 of Mitchner and Kruger (1973). Edgar et al. (1973) give cross sections for five ionization continua of N_2 due to electron impact, with cross sections of 10^{-16} to 10^{-17} cm^2 at 100 eV. The cross sections are smaller by about a factor of three at 35 eV and decline rapidly at still lower energies. (The first ionization potential of N_2 is 14.5 eV.) Similar behavior is expected for other candidate dominant constituents of planetary atmospheres. For N_2 , below about 20–30 eV typical inelastic cross sections are of order 10^{-16} cm^2 down to about 1.5 eV, with variations of a factor of a few (e.g., the local peak at about 2 eV due to excitation of vibrational levels within the ground electronic states). Similar cross sections occur for other candidate molecules and for the thermal inelastic electron impact excitation of atoms inferred from data in Spitzer (1978). Taking this value of 10^{-16} cm^{-2} for the cross section, we estimate the inelastic collision frequency to be

$$\nu_{inel} = 5 \times 10^{-9} n \sigma_{inel,16} E^{1/2} \text{ sec}^{-1}, \quad (11)$$

where E is in eV, n is in cm^{-3} , $\sigma_{inel,16}$ is in units of 10^{-16} cm^2 . Comparing Eqs. 9 and 11 we find that inelastic excitation will dominate Coulomb thermalization ($\nu_{ee} \ll \nu_{inel}$) when

$$n_e/n \ll 4 \times 10^{-2} \sigma_{inel,16} E_{35}^2, \quad (12)$$

where E_{35} is in units of 35 eV. According to Crisp (2000), the ionization fractions in the D (~ 90 km), E (~ 110 km), F1 (~ 170 km) and F2 (~ 300 km) layers of the Earth's ionosphere are only 10^{-12} , 10^{-7} , 10^{-5} , and 10^{-3} , respectively. As our results will show, all but the most extreme cases of irradiation (such as a 10^8 erg cm^{-2} stellar flare) will produce ionization fractions below the limit

of Eq. 12. Thus *the secondary electrons will expend nearly all their energy in excitation, and almost none in heat.*

Another portion of the secondary electron energy will be expended in elastic, electron-neutral, molecular collisions. The electric field of the electron polarizes the charge distribution in the molecule, inducing a dipole moment, leading to an effective potential at large distance that varies as r^{-4} and a cross section that varies as w^{-1} (recall w is the relative velocity). The calculated and measured momentum transfer cross sections for such interactions are large, of order 10^{-15} cm^2 at the energies of interest (10 times larger than for inelastic collisions). Despite the large cross section, the fractional energy lost by the secondary electron in a typical electron-neutral collision is of order $2m_e/Zm_p$ (e.g., Mitchner and Kruger 1973 Eq. 7.5), which makes this process much less than a 1% effect compared to excitation, and so we neglect it.

2.3.3. Approximate treatment of UV reemission

Although the secondary electrons have a distribution of energies, their mean energy is 35 eV for N_2 , a value which is known to be nearly independent of the composition, as discussed above. The electron excitation cross sections as a function of energy for N_2 have broad maxima around 10–80 eV (Jones 1974, Fig. 4.15), which neatly brackets the average energy of the secondary electrons, so we expect the collisionally excitable N_2 electronic states to be well populated among the target molecules. This suggests that, in the UV, the sources of strong reradiation will be N_2 emission bands, similar to the case for auroral lines (Jones 1974). Data for some of the more important band systems are given in Table 1 (Banks and Kockarts 1973; Lofthus and Krupenie 1977; Huber and Herzberg 1979). We emphasize that we have chosen a pure N_2 atmosphere simply to keep the calculations and presentation manageable, and that any molecule which might be suspected to dominate the compositions of terrestrial-like exoplanet atmospheres has similarly spaced electronic levels and should be excited with comparable efficiency.

We ignore the complication of the full line radiative transfer, since we are interested in only estimating the transparency of atmospheres to auroral emissions. The density and amplitude of

Transition	Species	Wavelength range
$\text{A}^3\Sigma_u^+ - \text{X}^1\Sigma_g^+$ (Vegard-Kaplan)	N_2	210–540 nm
$\text{a}^1\Pi_g - \text{X}^1\Sigma_g^+$ (Lyman-Birge-Hopfield)	N_2	130–200 nm
$\text{E}^3\Sigma_g^+ - \text{A}^3\Sigma_u^+$ (Herman-Kaplan)	N_2	213–274 nm
$\text{C}^3\Pi_u - \text{B}^3\Pi_g$ (2nd positive)	N_2	268–545 nm
$\text{B}^2\Sigma_u^+ - \text{X}^2\Sigma_g^+$ (1st negative)	N_2^+	320–600 nm

Table 1: Strongest UV N_2 and N_2^+ electronic band systems (Banks and Kockarts 1973; Lofthus and Krupenie 1977; Huber and Herzberg 1979).

lines (in photon number per unit wavelength) in auroral spectra is roughly distributed uniformly from the UV to the near IR (see spectra in Jones 1974; Chamberlain 1961), so we assume the energy fluence $F_{\text{dep},i}$ deposited at each layer i is reradiated from that layer in the form

$$\frac{dF_{\text{UV},i}}{d\lambda} = \frac{F_{\text{dep},i}}{\lambda \ln(\lambda_{\text{max}}/\lambda_{\text{min}})} \quad (13)$$

between the wavelengths λ_{min} and λ_{max} corresponding to the lower and upper limits of the important auroral emission lines. The Monte Carlo calculation yields the fraction of the original incident energy that is deposited by X-ray photoabsorption and Compton recoil at each layer i . From this number, we assume that all primary electron energy is transferred to secondary electrons. At each layer a spectrum of the form of Eq. 13 is reemitted isotropically and then attenuated either by Rayleigh scattering or molecular absorption.

We have replaced the rich and extremely complex line spectrum of N_2 (and other molecules) by a continuous spectrum that contains (roughly) the same amount of flux per unit wavelength interval as the line spectrum. This smearing of the line spectrum into an equivalent continuous spectrum was assumed because: (i) we are interested in only an order-of-magnitude estimate for the fraction of energy that reaches the ground in each wavelength interval, and (ii) the alternative would require the solution of a large number of rate equations for the level populations at each altitude, a calculation beyond the scope of the present work.

2.3.4. Atmospheric UV screening

Any UV reemission will be subject to a variety of opacity sources within the exoplanet atmosphere. Depending on the precise atmospheric composition, the primary UV screens might be molecular absorbers or aerosols, or in the absence of these, pure Rayleigh scattering. We take two extreme limits: pure O_3/O_2 absorption with a terrestrial abundance profile (characteristic of present-day Earth) and pure Rayleigh scattering (i.e., no molecular or aerosols absorbers, characteristic of Archean Earth). Although we recognize that there is considerable uncertainty concerning UV screening in the Archean atmosphere (e.g., Levy and Miller 1998; Cockell 2002), recent evidence concerning mass-independent isotopic fractionation in Archean sulfides (Farquhar et al. 2002) suggest the absence of a significant UV shield during this period (Wiechert 2002), so our assumed Archean atmosphere may not be so extreme. And if fluxes are large enough to significantly erode the ozone layer (e.g., Gehrels et al. 2003 and references therein), then the pure scattering case may be relevant even for periods when the planet possessed an ozone layer.

To find the fraction of the reemitted flux that would reach the ground in the case of pure Rayleigh scattering, we attenuated the reemission on a layer-by-layer basis according to a modification of the Schuster (1905) solution for “foggy” atmospheres, which is a special case of the two-stream approximation (see Appendix D for the full derivation). In this scheme, the fraction of

the flux emitted at layer i transmitted by the atmosphere is

$$T(\lambda, z) = \frac{1/2 + \tau_{\uparrow}(\lambda, z)}{1 + \tau_{\uparrow}(\lambda, z) + \tau_{\downarrow}(\lambda, z)}, \quad (14)$$

where τ_{\downarrow} and τ_{\uparrow} are the optical depths of the part of the atmosphere below and above the layer of reemission, respectively. We assume, to good approximation, that the emission layer itself is of negligible optical depth (we use 256 altitude zones per atmosphere). The redistributed UV flux received at the ground, F_{UV} , is then

$$F_{\text{UV}} = \int_0^{z_{\text{max}}} \int_{\lambda_{\text{min}}}^{\lambda_{\text{max}}} F_{\text{UV}}(\lambda, z) T(\lambda, z) d\lambda dz, \quad (15)$$

where $F_{\text{UV}}(\lambda, z)$ is the differential photon number spectrum as a function of wavelength and altitude, z_{max} is the altitude of the highest atmosphere zone, and $T(\lambda, z)$ is the wavelength-dependent transmission function for layer at height z given by Eq. 14 for the optical depths above and below that layer. The surface transmitted energy fractions we calculate in this manner are upper limits, since we neglect aerosol absorption and scattering and collisional deexcitations (see Appendix A).

A very different situation occurs if the atmosphere contains a significant source of UV molecular opacity at altitudes below the bulk of the secondary electron deposition. We use O_2 and O_3 as our prototype. To examine molecular absorption, we must neglect Rayleigh scattering, since the above treatment applies only in the pure scattering limit. We assume the transmission through each layer in the presence of molecular absorbers follows the Beer-Lambert law, so that

$$T(\lambda, z) = \exp[-\tau(\lambda, z)], \quad (16)$$

where $\tau(\lambda, z)$ is the wavelength-dependent optical depth to absorption from height z to the ground. The subsequent calculation of F_{UV} is analogous to Eq. 15. Integrating over atmospheric layers is equivalent to a formal solution to the transfer equation (neglecting the angular dependence), in which the source function at each layer is due only to redistributed UV radiation, since the thermal contribution at these wavelengths is negligible for any possible atmospheric temperature. For this case, we assume that half of the reemitted flux is directed straight downward and half is directed upward. We ignore the upward fraction and attenuate the downward half to obtain our estimate.

We chose terrestrial fractional abundances of O_2 and O_3 (taken from Brasseur et al. 1999 for altitudes up to 60 km and from Champion et al. 1985 for higher altitudes) for our absorption case. Since the relative ozone is to zeroth order a photoproduct of irradiation incident on the top of the atmosphere, the ozone concentrations as a function of column density from the top of the atmosphere should be approximately invariant. Taking ozone on the Earth as the prototype, we scaled terrestrial concentrations to match our various atmosphere models. In each case, the fractional abundance of ozone at a particular altitude on the exoplanet was matched with the abundance of terrestrial ozone at an altitude corresponding to the same column density from the top of the atmosphere. In cases where the exoplanet atmospheric column density was smaller than

that of Earth, we truncated the ozone profile at low altitudes. It must be noted that this is a gross simplification, since the O_3 profile depends on the O_2 column density, not the total optical depth, and even then the O_3 peak does not follow the O_2 column density linearly because of the density-dependence of the ozone production from $O + O_2$ (Kasting and Donahue 1980; Kasting et al. 1985). For this reason the calculations of ozone shielding of the redistributed UV radiation must be considered as illustrative only. The wavelength-dependent O_2 and O_3 cross sections were taken from Yung and DeMore (1999). The transmitted fractions in the presence of the ozone shield presented hereafter assume an upper limit to the biologically relevant flux of 320 nm. Unfortunately, the results are very sensitive to this quantity (as shown in Fig. 8), but evidence from terrestrial UV-B damage (see §3.3) supports this conservative value.

The effects of collisional deexcitation of target molecules is addressed in detail in Appendix A. We find that, for the strongest auroral nitrogen lines, this mode of energy dissipation is unimportant.

3. Results and discussion

3.1. Habitable exoplanet surfaces can be exposed to significant γ -ray—but not X-ray—fluences

According to our Monte Carlo calculation, exoplanet atmospheres with column densities between roughly 30 and 100 $g\ cm^{-2}$ (habitable by our definition in §2.1.1) will transmit at least 1% of the incident γ -rays to the surface. Furthermore, for atmospheres between 30 and 50 $g\ cm^{-2}$ and a source of MeV photons such as a supernova or gamma-ray burst, most of the surficial energy fluences will be due to the incident ionizing radiation. The characteristic energy of the radiation received at the ground on planets with thin atmospheres will be very high since the redistribution of the radiation through electron-mediated excitation processes discussed above will be small due to the low optical depths.

Even in thin atmospheres, the surficial spectrum will be altered from the incident spectrum. The relevant physics can be summarized as follows. A photon will typically start with a very high energy (1 MeV, say) and lose a significant fraction of its energy to Compton recoil electrons at each interaction. This fraction depends on energy and decreases with decreasing energy, leading to a “pile-up” of photons at energies of $\lesssim 100$ keV. In the low-energy limit ($E \ll m_e c^2$), the average energy shifts are well-approximated by $\langle \Delta E \rangle \simeq E^2$ (obtained by averaging the Compton energy losses weighted by the angular Klein-Nishina cross section). The photons at successively lower energies experience a photoabsorption cross section that increases rapidly ($\sigma_{pa} \propto E^{-3}$) and are thus removed from the Compton downscattering peak. This is demonstrated in Fig. 1, which shows the energy spectra at the surface for four different column densities and an incident energy of 1 MeV. The downscatter ledge, where the photons are “piling up,” can be seen (~ 50 –100 keV) along with a continuum of energies between this peak and the maximum incident energy. This continuum is filled by photons that lost a smaller than average energy at one or more Compton scatterings.

Also seen for the thinnest atmospheres are the peaks at the average energies corresponding to both one and two Compton scatterings from an initial energy of 1 MeV.

For stellar flare spectra, energies are in the keV range, and the dominant cross section is photoabsorption, and no downscattering occurs. Figure 2 shows the effect of atmospheric attenuation on an incident stellar flare model spectrum, represented by a decaying exponential with average energy of 10 keV. Unlike the γ -ray case, the X-ray flare spectrum actually shifts to higher mean energies than the incident spectrum because the flux is attenuated primarily according to the photoabsorption cross section, which is proportional to E^{-3} . The estimated fraction of ionizing radiation received at the ground for exoplanets with thin atmospheres is shown in Fig. 3. Interestingly, since the surficial radiation spectrum has such high characteristic energies for the thinnest atmospheres, the transmittance is nearly independent of atmospheric composition (i.e., the primary photon reprocessing occurs through Compton scattering, which is independent of composition). This makes our results quite general if indeed exoplanets with such thin atmospheres are habitable.

Even in the optically thin limit, a finite amount of energy redistribution to the UV occurs. As stated above, the γ -rays dominate the surface spectrum for atmospheres with column densities between 30 and 50 g cm⁻²; above this range, the UV reemission dominates on planets without an atmospheric screen. Figure 3 shows the relative contributions of the incident radiation and the reemission to the fraction of incident energy received at the ground in the two extreme cases of Rayleigh scattering and absorption by an O₂/O₃ UV shield similar to the terrestrial O₃ distribution with optical depth scaled as described earlier. Even when subjected to an O₂/O₃ screen, the transmitted UV reemission still exceeds the directly transmitted ionizing radiation for column densities above about 100 g cm⁻², and the transmitted fraction is about 1% at that column density.

3.2. Secondary ionospheric layers can be produced

To justify our neglect of ion recombination on generic terrestrial-like exoplanets, we must examine the most extreme cases of irradiation. A supernova at a distance of 1 pc—which should occur very rarely, if at all, during the lifetime of a planetary system—would yield a maximum fluence of about 10⁸ erg cm⁻² of ionizing radiation (hard UV and X-rays from shock breakout and γ -ray lines); a 10³⁵ erg superflare of a solar-type star would give a slightly smaller fluence for a planet at 1 AU, while a 10³⁴ erg dMe flare gives a somewhat larger fluence for a planet in the conventional habitable zone (~ 0.1 AU distant for such a low mass star). These extreme events would generate electron fractions smaller than the limit given above in Eq. 12, even neglecting recombination. The vast majority of events will easily satisfy that strong inequality, especially if recombination timescales are not much larger than the duration of the irradiation events. We are thus able to obtain a reliable estimate of the maximum ionization fractions caused by astrophysical irradiation while neglecting recombination.

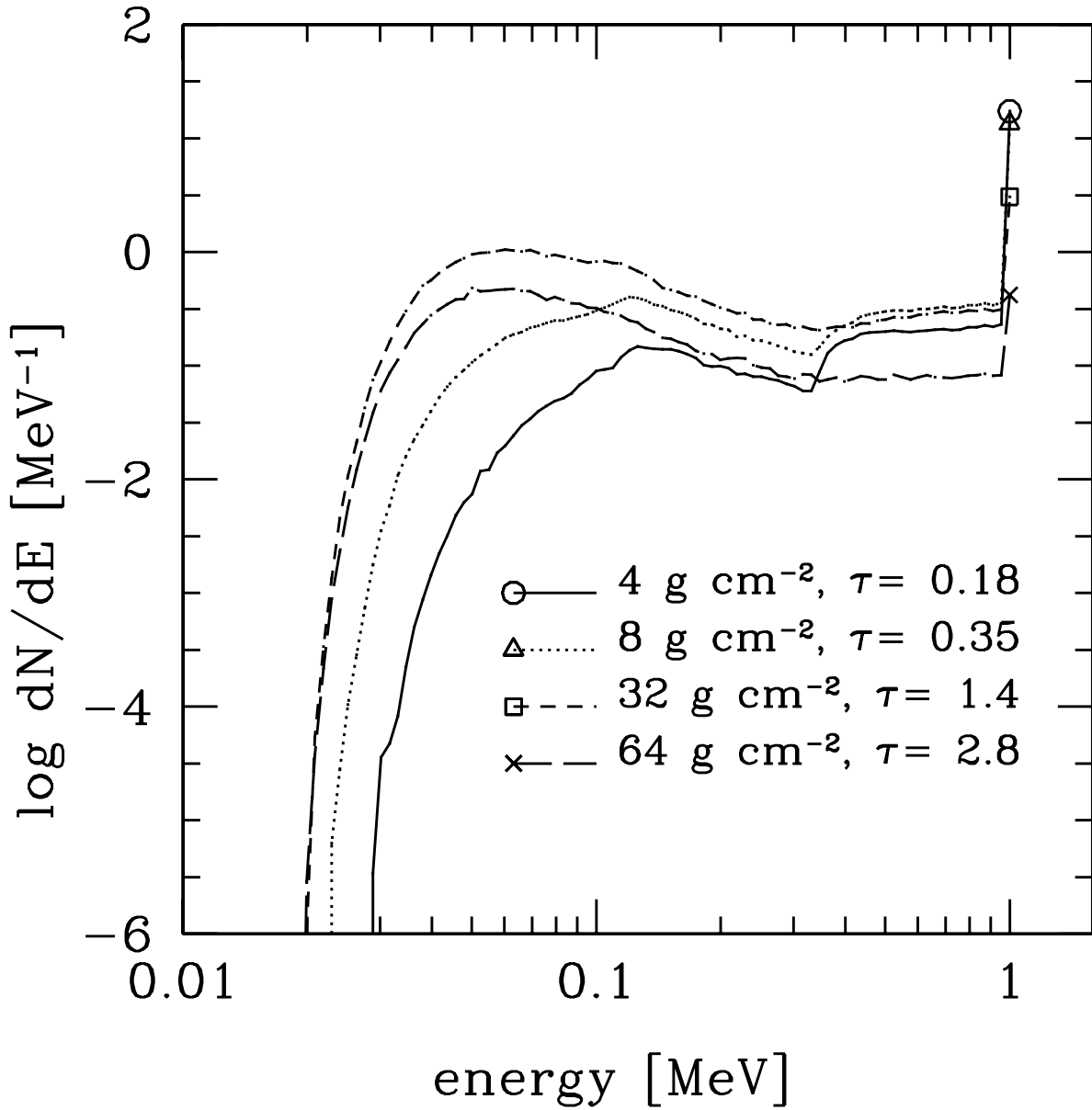


Fig. 1.— Spectra of the ionizing radiation received at the ground for four thin atmospheres and a 1 MeV monoenergetic incident spectrum. The Compton backscattering peaks for the first and second scatterings starting at 1 MeV can be seen for the two thinnest atmospheres, as well as the “piling up” at 50–100 keV due to successively smaller energy shifts.

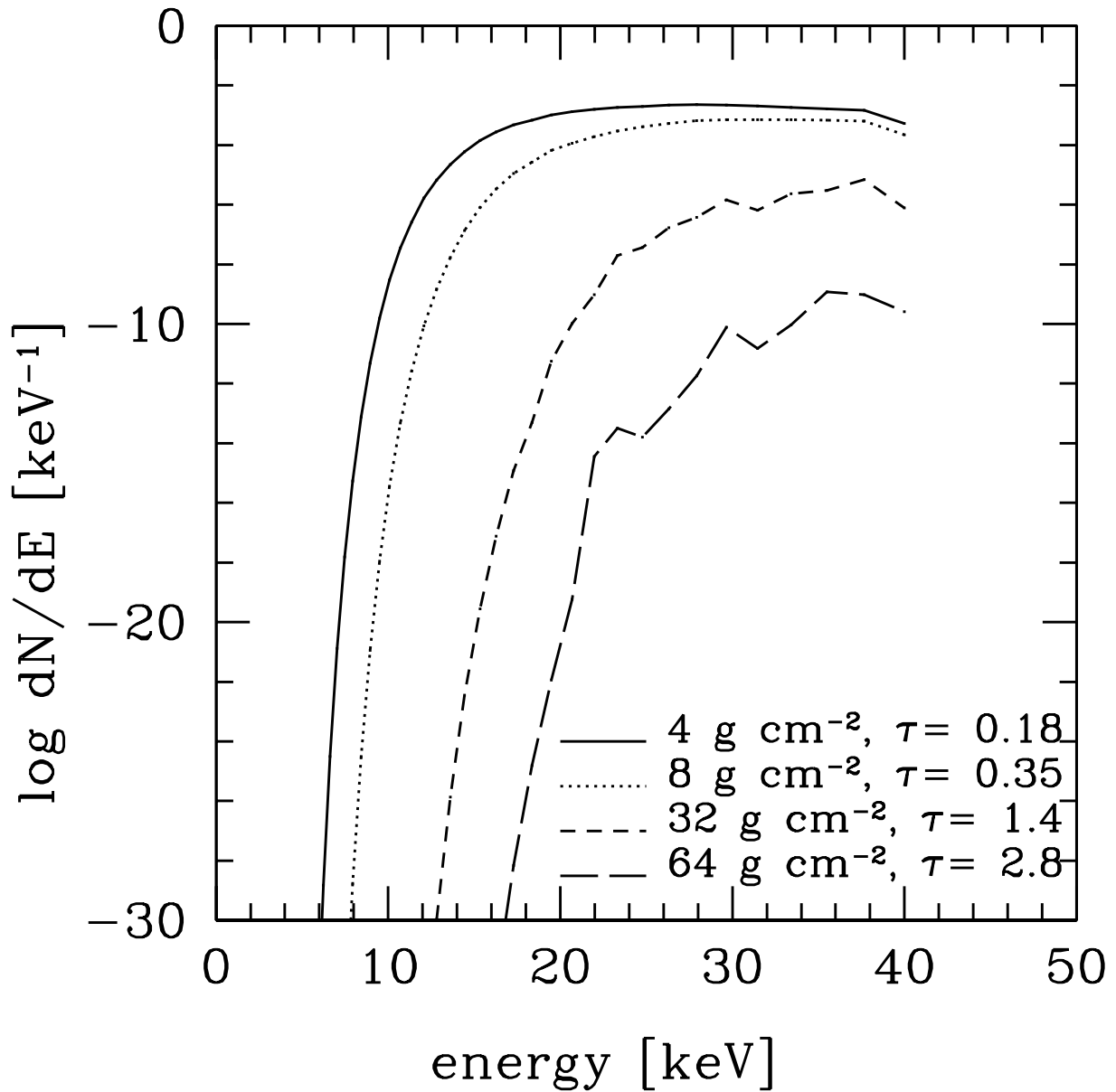


Fig. 2.— Spectra of the radiation received at the ground for four thin atmospheres and an exponential incident spectrum with an average energy of 10 keV.

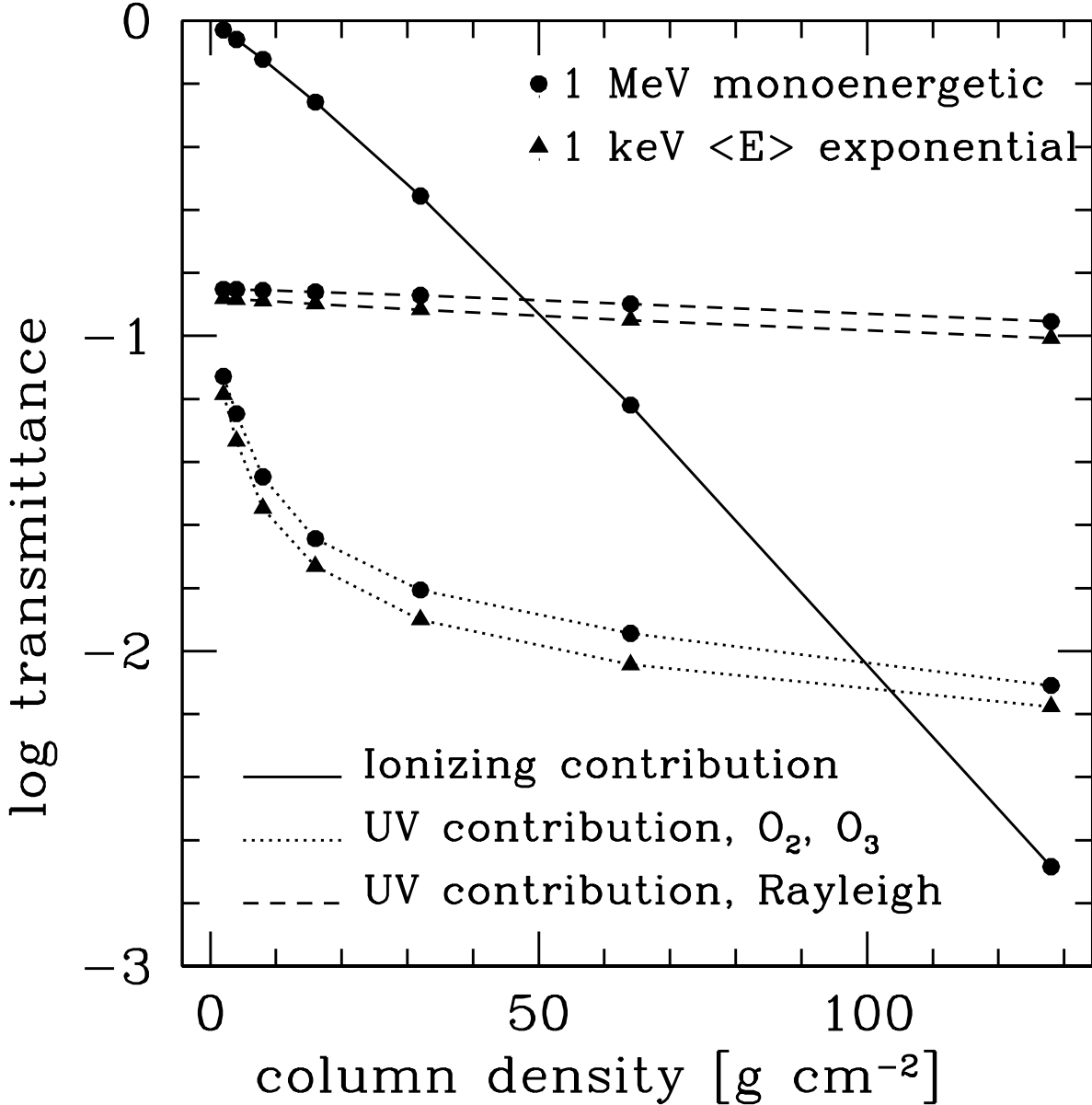


Fig. 3.— Fraction of the incident energy reaching the ground as ionizing radiation and as biologically effective UV in thin atmospheres for two incident spectra using two simple models of UV redistribution. The ionizing radiation dominates for column densities $\lesssim 50 \text{ g cm}^{-2}$ for hard incident radiation. For the softer, $\langle E \rangle = 1 \text{ keV}$, case, photoabsorption prevents any substantial direct surficial flux; we omit the solid curve corresponding to the X-ray incident spectrum because the transmittance is far below the scale shown here. The UV reemission contribution is shown for two cases: (1) O_2 and O_3 molecular absorption only and (2) Rayleigh scattering only. In both UV cases, only the biologically effective flux (200–320 nm) is counted.

Even with moderate levels of irradiation, regions of the terrestrial-like exoplanet atmosphere can be ionized to the level of the terrestrial ionosphere. For comparison, the ionization fractions in the terrestrial ionospheric D and E layers are 1×10^{-12} and 1×10^{-7} (Crisp 2000), respectively. The ionization profiles we calculate show nearly constant ionization levels for the monoenergetic spectra down to a characteristic altitude, below which the ionization level drops extremely rapidly. For our continuous spectra, ionization levels rise with increasing altitude because the photon number per unit energy decreases with increasing energy. Thus most photons in our continuous spectra have lower energies (and larger interaction cross sections) than the spectrum average and will be deposited at higher altitudes. Figure 4 shows the results for a few atmosphere models. Even for atmospheres as thick as Earth’s, the ionization profiles shown as fractional ionization produced per unit incident fluence for γ -ray incident spectra show a significant effect down to altitudes below the lowest steady-state ionization layer on Earth (D layer, 60–95 km; Crisp 2000). For example fluences at the top of the atmosphere of 1 erg cm^{-2} from a stellar flare with average energy of 10 keV would be yield a transient layer of comparable ionization fraction to the D layer, but at much lower altitudes. Based on this result, we predict that additional ionization layers may be produced on a transient basis and with stochastic ionization levels in response to external radiation sources. Neglecting recombination, the maximum ionization fractions per unit incident fluence (hereafter, ionization efficiency) are independent of column density, depending only on the incident spectrum. For stellar flare irradiation with hard X-ray spectra of average energy in the range 1–10 keV, we find maximum ionization efficiencies of 10^{-5} – 10^{-7} (erg cm^{-2}) $^{-1}$; for supernovae and gamma-ray bursts, we find maximum ionization efficiencies of 10^{-12} – 10^{-13} (erg cm^{-2}) $^{-1}$. Maximum ionization efficiencies as a function of average incident energy are shown in Fig. 5.

As the ionization fraction at a particular layer depends on the amount of energy deposited in that layer, it is instructive to examine the energy deposition profiles, defined here as the variation in the fraction per km of the incident energy transferred to photoelectrons and Compton recoil electrons as a function of altitude. Figure 6 shows that our model stellar flare spectrum deposits more energy at higher altitudes than the corresponding monoenergetic incident spectrum at the same average energy. This has important implications for the ionization fractions created. Because the density of atmospheric molecules falls off exponentially with height, a higher fraction of energy deposited at higher altitudes where molecular densities are lower will result in higher ionization fractions. This is why the stellar flares may create higher peak ionization fractions than supernovae, and why the altitudes of peak ionization will be higher.

3.3. Substantial diffuse UV is produced in thick atmospheres

We can estimate the intensity of aurora-like emission produced by superflares and cosmic explosions here and on other planets by comparing with terrestrial data. Auroral intensities are often classified into four “International Brightness Coefficient” (IBC) Classes I–IV, from weakest to strongest. According to data presented by Whalen et al. (1985) for IBC Class III auroral intensities,

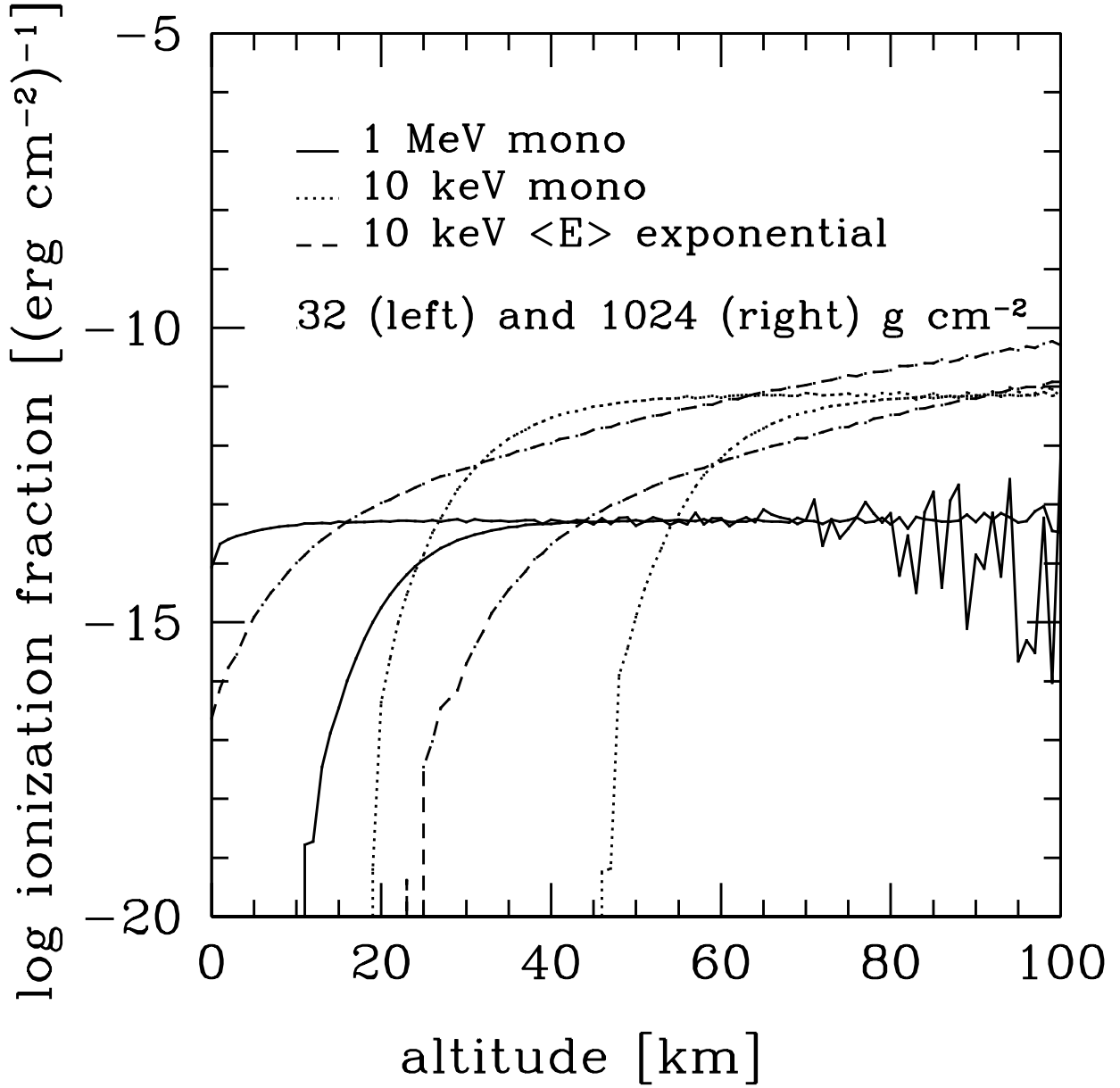


Fig. 4.— Typical ionization efficiency profiles (neglecting recombination) for three different incident spectra and two column densities. Vertical units are ionization fraction produced per cm^3 per unit incident fluence at the top of the atmosphere. For monoenergetic spectra, nearly constant ionization levels are produced down to a characteristic altitude, which roughly corresponds to the altitude of maximum energy deposition. This agrees well with the Chapman solution. The model flare spectra produce ionization levels which rise with increasing altitude because more energy is deposited at higher altitudes than in the monoenergetic case with an identical average energy. The progressively larger fluctuations at altitudes above ~ 60 km are due to small-number statistics, where the optical depths are small and photon interactions are statistically unlikely.

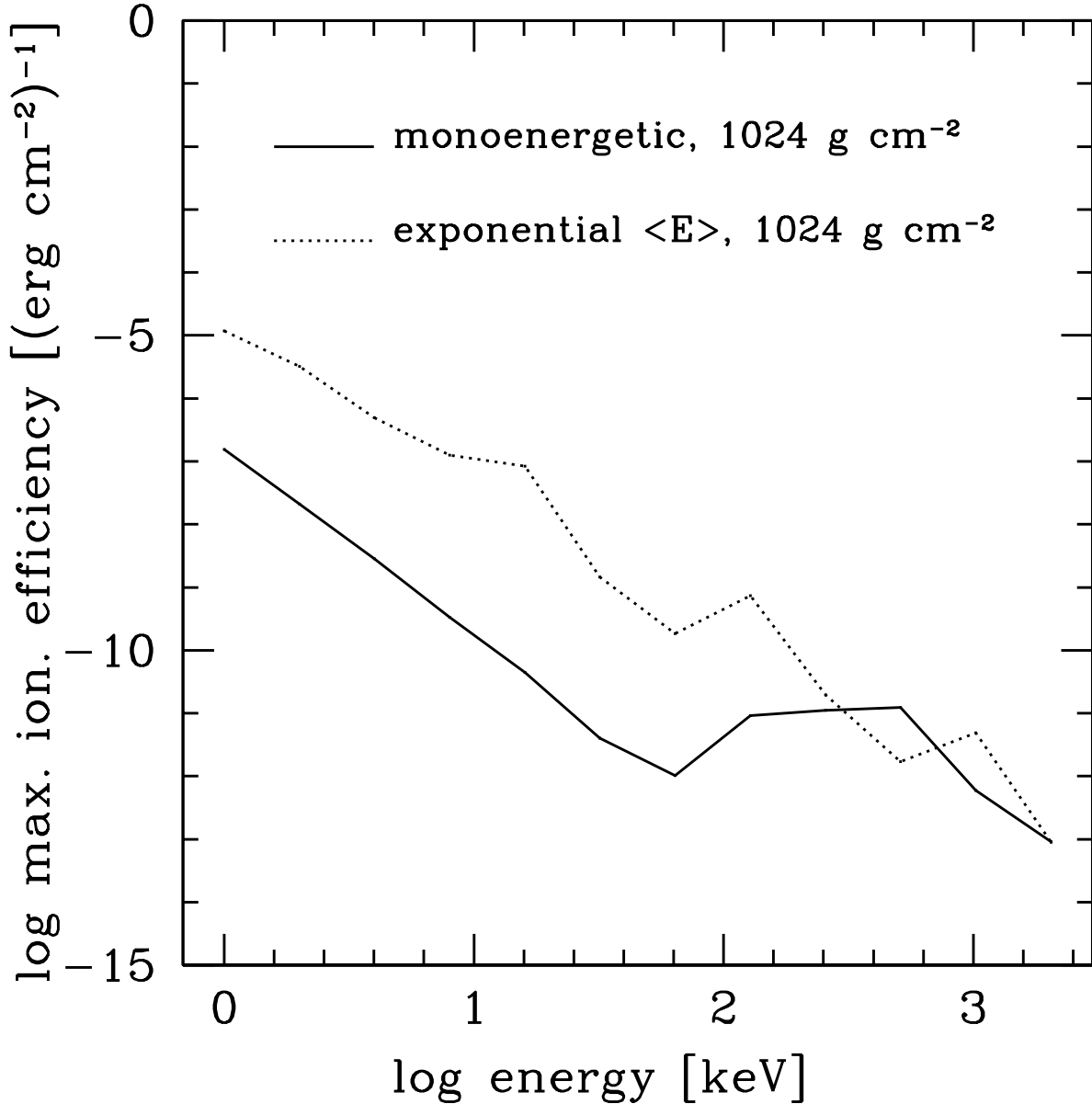


Fig. 5.— Maximum ionization efficiencies (fractional ionization produced per unit fluence of incident energy) for average incident energies between 1 keV and 2 MeV and a column density of 1024 g cm^{-2} . The efficiency declines as energy increases because most of the energy is being deposited at lower altitudes where molecular number densities are higher and hence a given amount of energy is able to ionize a smaller fraction of the molecules. Uncertainties in the curve arise from small-number statistics—only a small fraction of the incident photons are interact in the layer of maximum energy deposition, creating fluctuations in the altitude of maximum ionization.

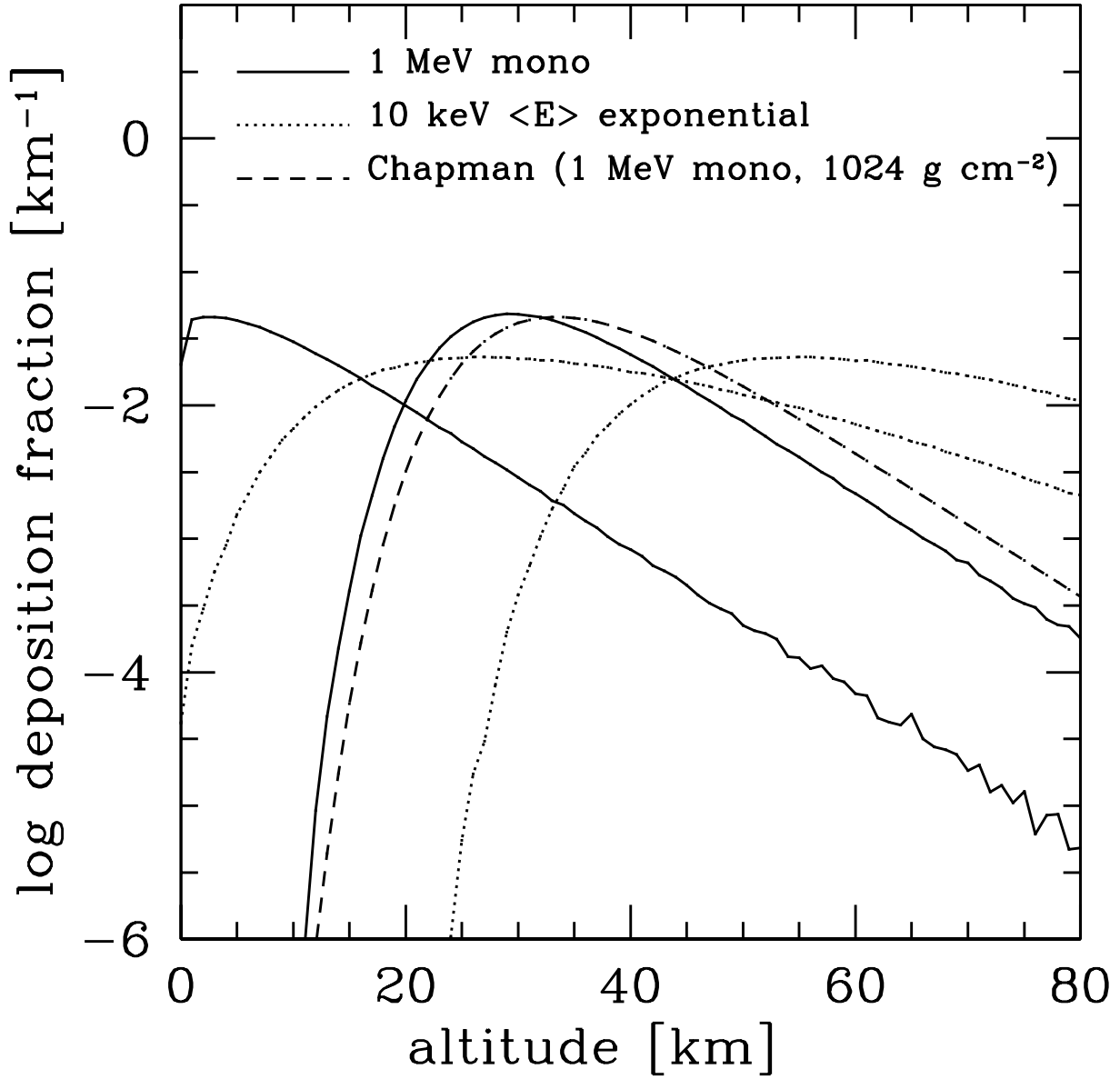


Fig. 6.— Energy deposition profiles for three different incident spectra in atmospheres with column densities of 32 and 1024 g cm^{-2} . For each spectrum, the lefthand curve is for a 32 g cm^{-2} column density and the righthand curve is for a 1024 g cm^{-2} column density. A single curve corresponding to the Chapman solution for a 1 MeV monoenergetic incident spectrum in a 1024 g cm^{-2} atmosphere is shown for comparison. Note that our Monte Carlo results for the monoenergetic spectra are identical in shape to the Chapman solution (which assumes a monoenergetic incident spectrum) except for a shift to lower altitudes which accounts for the effects of multiple scattering. Also it can be seen that continuous spectra give different overall shapes, with our model flare spectrum depositing more energy higher in the atmosphere than a monoenergetic spectrum at the same average energy.

the OI 557.7 nm emission is about 1% of the total zenith auroral brightness. For the most intense auroral events with IBC Class IV the brightness in the OI line is 10^{12} photons $\text{cm}^{-2} \text{s}^{-1}$. Using the same scaling from OI to total brightness as for the Class III event, the total brightness must be of order 10^{14} photons $\text{cm}^{-2} \text{s}^{-1}$. Using 5 eV as a median energy photon for the auroral emission, this gives a rough energy flux of 8×10^2 erg $\text{cm}^{-2} \text{s}^{-1}$. For the Class III data, the efficiency of conversion of primary and secondary electron energy into radiation at all wavelengths is given to be 21–35%, so the corresponding photon flux for the Class IV event is about 3×10^3 erg $\text{cm}^2 \text{s}^{-1}$. We find larger efficiencies for the ratio of incident photon energy to electron energy for the very different physical process producing the electrons here (Compton scattering and photoabsorption, versus collisional ionization for standard aurorae), and similar efficiencies can be inferred from calculations of X-ray redistribution in accretion disks around compact stellar objects (Ross 1979; Kallman and McCray 1982; Ross and Fabian 1993).

In comparison to these terrestrial events, we have estimated that gamma-ray burst events (Scalo and Wheeler 2002) and supernova explosions (Scalo et al. 2003) would expose an exoplanet to incident ionizing fluences greater than 10^6 erg cm^{-2} hundreds of times per Gyr, which translates to fluxes of about 10^7 erg $\text{cm}^{-2} \text{s}^{-1}$ and 10^2 erg $\text{cm}^{-2} \text{s}^{-1}$, respectively. On a planet orbiting a low-mass dMe strong flare star in the habitable zone (semimajor axis ~ 0.1 AU), a flare with an EUV energy greater than 10^{32} erg can occur 10–100 times per day (see Audard et al. 2000, Fig. 4), with a corresponding flux for a 10 minute flare of 6000 erg $\text{cm}^{-2} \text{s}^{-1}$. Given the energy-frequency power law relations estimated for both solar (e.g., Crosby et al. 1993 and Aschwanden et al. 2000) and dMe flares in various UV and X-ray bands (Gershberg and Shakhovskaya 1983; Audard et al. 2000; Güdel et al. 2003), with differential frequency distributions of -1.5 to -2.2 , incident fluxes of at least 10^5 erg $\text{cm}^{-2} \text{s}^{-1}$ should occur with a frequency of order once per day. Clearly the intensities of auroral lines generated by these events will far exceed the strongest terrestrial Class IV auroral displays.

Figure 7 shows the fraction of the incident fluence reaching the surface in the biologically significant range 200–320 nm for column densities up to 2048 g cm^{-2} . The original incident radiation is strongly attenuated, but the redistribution of energy toward UV emission maintains the surface fluences at significant levels. Two cases are shown: pure Rayleigh scattering and pure O_2/O_3 absorption. The pure Rayleigh scattering case represents an atmosphere with no significant molecular or aerosol UV absorbers in the biologically effective region—perhaps similar to the Archaean Earth. The transmission in this case was calculated using the modified two-stream Schuster (1905) scattering solution described in Appendix D. The O_2/O_3 case represents an ozone and oxygen abundance similar to the present-day Earth (identical column density profiles). As can be seen in Fig. 7, the effect of redistribution to the UV is quite dramatic, even when subjected molecular absorption by O_2 and O_3 . The UV reemission quite effectively raises the surficial fluences back to significant levels, even though the incident ionizing radiation has been attenuated to ridiculously small amounts in the thick atmospheres. For example, the fraction of incident X-rays and γ -rays reaching the surface on Earth (1024 g cm^{-2}) is 6×10^{-29} for the 1 MeV monoenergetic case, while

including the UV redistribution to the biologically relevant 200–320 nm region, even in the presence of an ozone screen, raises this number to at least 2×10^{-3} .

The results depicted in Fig. 7 depend sensitively on the adopted upper limit of 320 nm for “biologically effective” UV radiation, but we feel that a value of 320 nm is quite reasonable. Figure 8 shows the strong dependence of the transmission on the adopted upper wavelength limit for “biological significance.” For the case of O₃ absorption, the dependence is quite severe, so the transmission will depend on which specific biological process is of interest. It is well known that UV-B radiation around 320 nm has major effects on contemporary organisms and ecosystems, and even wavelengths as large as 350 nm can have a variety of biological effects (e.g., Jagger 1985). For example the action spectrum for induction of squamous cell carcinoma in mice has a strong peak at 300 nm and is smaller by only an order of magnitude at 320 nm (Nilsson 1996, p. 88). Additionally, UV-B (280–315 nm by convention) can penetrate ocean surfaces to much larger depths than UV-C (100–280 nm). Although many DNA action spectra peak at 260 nm and have declined by a factor of 10–100 by 300–320 nm, the action spectrum for particular *mutations* do not show this universal behavior. As one of many well-known examples, the measured action spectrum for the UV-induced mutation to resistance to novobiocin in *Haemophilus influenzae* has a sharp peak around 330 nm and drops by two orders of magnitude below 280 nm and above 360 nm (Cabrera-Juarez and Setlow 1976). A recent survey of the numerous effects of the longer-wavelength UV-B radiation on terrestrial organisms and ecosystems is given by Paul and Gwynn-Jones (2003).

3.4. Additional considerations

3.4.1. The Chapman solution is inaccurate for thin atmospheres and high energies

The problem of energy deposition in an exponential atmosphere for the case of pure absorption was solved by Chapman (1931). While our situation is more complicated, the photons are nevertheless depositing energy in the atmosphere, and we can compare our results to Chapman’s solution, which is commonly used to estimate the effects of ionizing radiation (e.g., Gehrels et al. 2003). Assuming an exponential attenuation in an exponential atmosphere, Chapman showed that the energy deposition rate, q , as a function of altitude is (see Chamberlain 1978)

$$q(y) = q_{\max} \exp(1 - y - e^{-y}), \quad (17)$$

where $y = (z - z_{\max})/h$ is the dimensionless altitude, z_{\max} is the altitude of maximum deposition, and h is the atmospheric scale height. This solution is based upon an exponentially increasing optical depth, so that the attenuation of the radiation (and hence the energy deposition) follows the profile of an exponential raised to an exponential. Additionally, the altitude of maximum deposition in the Chapman solution scales logarithmically with the optical depth:

$$z_{\max} = h \log \tau. \quad (18)$$

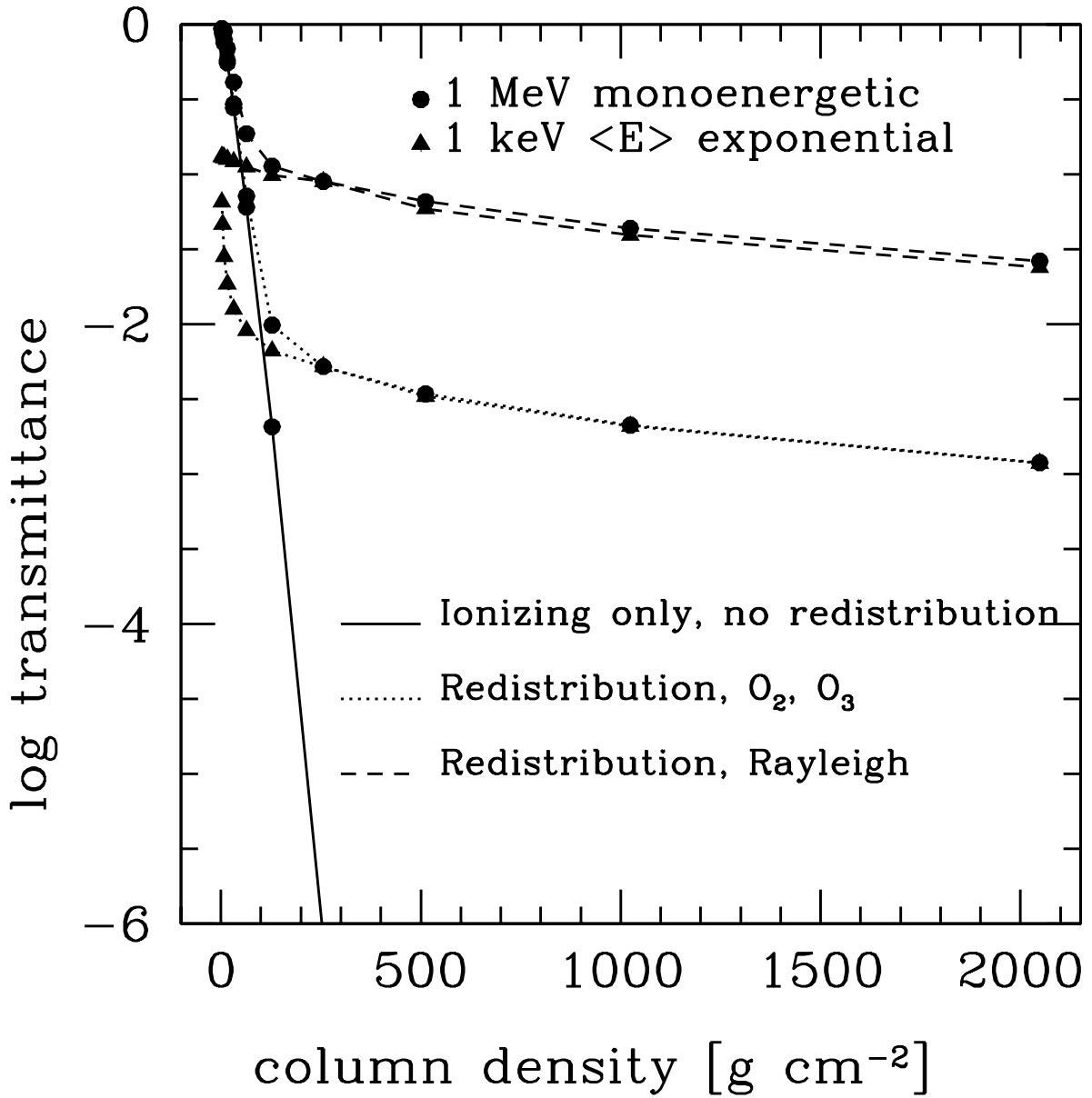


Fig. 7.— Fraction of the incident energy reaching the ground is shown both without and with the additional contribution of the redistributed UV for two simple models of UV redistribution for an atmosphere with a column density of 1024 g cm⁻². The no redistribution case for a 1 keV average energy exponential spectrum is not shown because the transmitted fraction is practically zero.

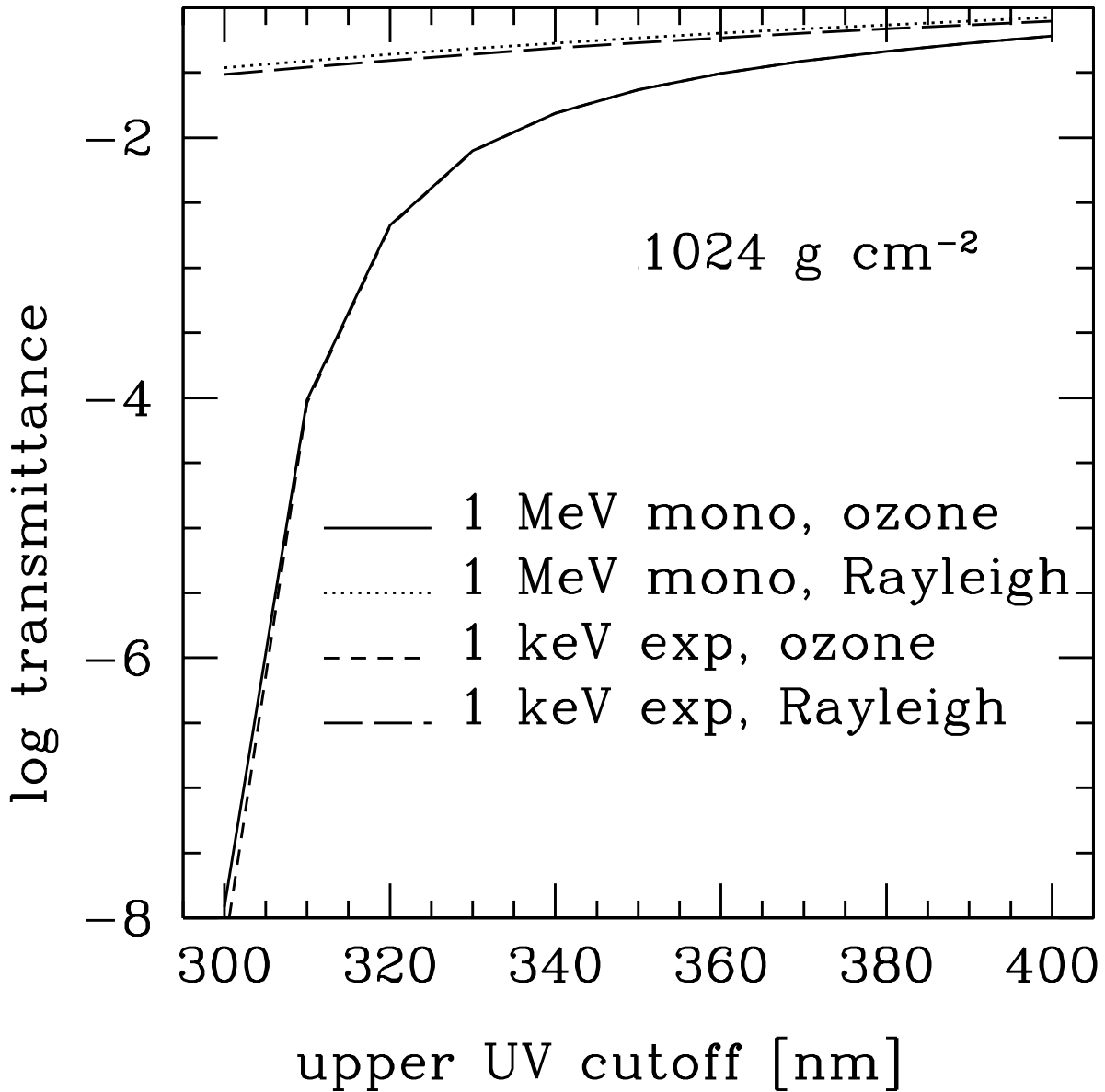


Fig. 8.— Fraction of biologically significant redistributed UV energy that is reaching the ground on Earth as a function of the upper cutoff for the biologically significant flux. The lower limit is taken to be 200 nm in all cases. The result is insensitive to the cutoff for the Rayleigh scattering case, but very sensitive in the O_3 case for cutoffs in the range 300–340 nm. The sharp falloff in the O_3 case for wavelengths shorter than 340 nm is due to the rapidly increasing O_3 cross section at smaller wavelengths (peaking around 260 nm). Significant biological effect occurs up to 350 nm in some organisms under UV irradiation. Our work assumes 320 nm for the cutoff.

Our Monte Carlo results, which take into account multiple scatterings, yield an energy deposition curve which is of the same shape as that which the Chapman solution (which assumes a monoenergetic incident spectrum) predicts, but with the entire curve shifted to lower altitudes due to the effects of multiple scattering. This is evident in Fig. 6. Also it can be seen that continuous spectra give different overall shapes, with our model flare spectrum depositing more energy higher in the atmosphere than a monoenergetic spectrum at the same average energy. In principle, the shape of the energy deposition curve for the continuous spectrum could be retrieved via the Chapman solution by summing appropriately weighted Chapman curves at each energy in the range of energies in the continuous spectrum.

In short, the general shape of the Chapman profile is accurate at one particular energy (and hence for our monoenergetic supernovae spectra), but it underestimates how far into the atmosphere the radiation will penetrate because of the neglect of multiple scattering. This effect is minor for the thickest atmospheres (column densities $\gtrsim 300 \text{ g cm}^{-2}$) but becomes significant for thinner atmospheres (column densities $\lesssim 300 \text{ g cm}^{-2}$).

To gauge the effect of multiple scatterings in our Monte Carlo model, we calculated (Fig. 9) the fraction of the atmosphere above the height of maximum energy deposition, which is a measure of how far the radiation has penetrated the atmosphere. The effects of lower deposition altitudes are more pronounced for thinner atmospheres and higher energies. More scatterings occur before the photons are photoabsorbed for higher incident energies, and each scattering has a longer mean free path in thinner atmospheres. In terms of the fraction of the atmospheric mass penetrated by the radiation, the full radiative transfer yields 10–50% greater penetration, depending on the thickness of the atmosphere and the energy of the incident radiation. At low energies the photoabsorption dominates, so the results approach the Chapman solution. The Chapman monoenergetic solution could be used to build up solutions for continuous spectra, so it is not invalid for incident spectra such as flares or gamma-ray bursts. The key quantity is the average energy of the spectrum and the thickness of the atmosphere. The most pathological situation for the Chapman solution is a high-energy radiation source (e.g., supernovae and gamma-ray bursts) incident on a thin atmosphere ($\lesssim 100 \text{ g cm}^{-2}$).

3.4.2. *Surface energy fluences are not sensitive to the angle of incidence*

We find that decreasing the angle of incidence can measurably decrease the surface fluence of the *original* incident radiation, with the effect becoming quite significant for the highest energies ($\gtrsim 1 \text{ MeV}$) and thickest atmospheres ($\gtrsim 500 \text{ g cm}^{-2}$). Though in our model we assume normal incidence for every photon, the surface of a real exoplanet subjected to a source at astronomical distances will observe a point source with varying zenith distances, depending on the viewing geometry. This effect means that we have calculated only an upper limit to the direct transmittance of the atmospheres to the incident *ionizing* radiation. We note that this ionizing radiation is already insignificant in a biological sense for column densities greater than about 100 g cm^{-2} . As found

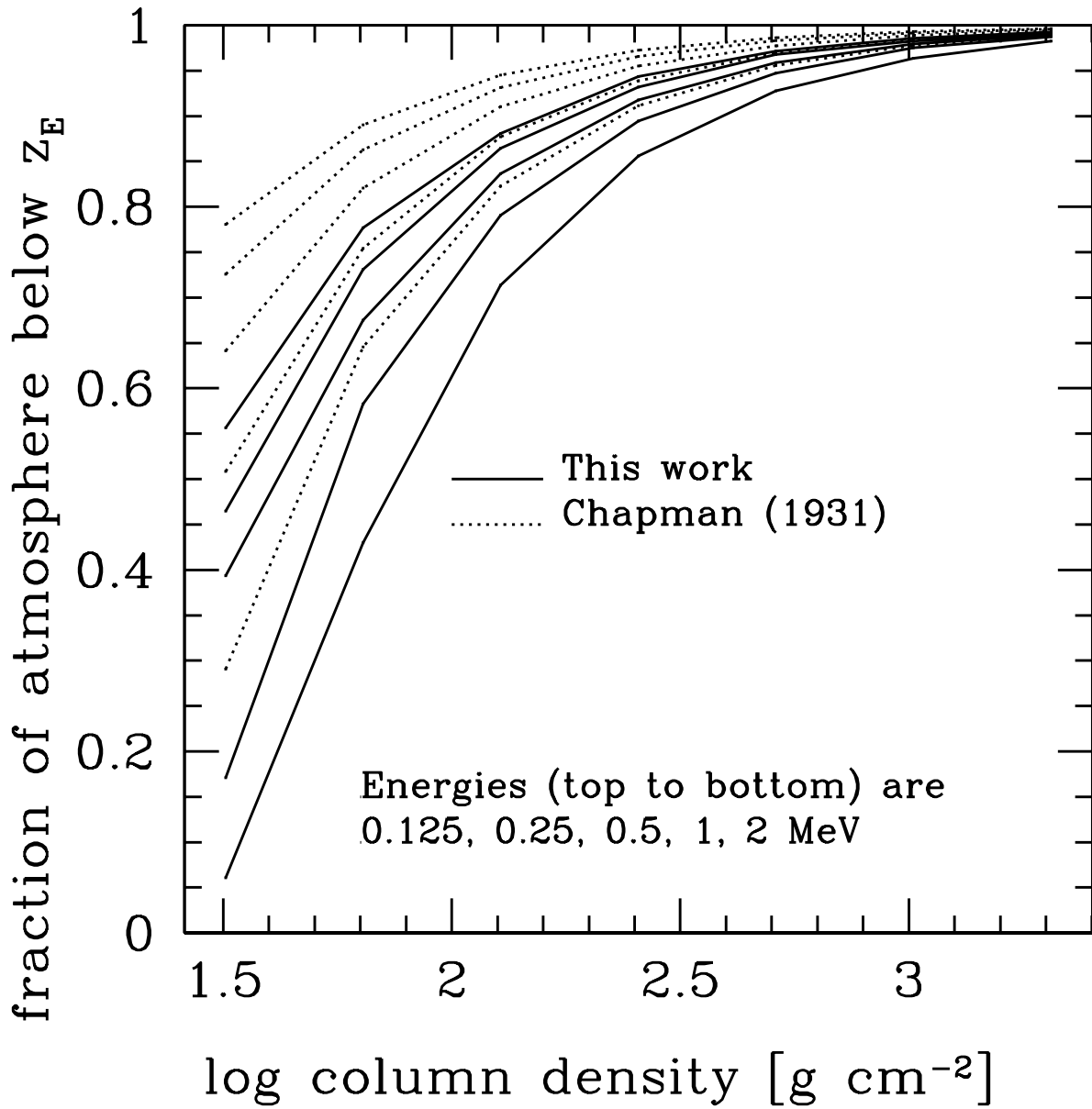


Fig. 9.— Comparison of the calculated location of peak energy deposition of monoenergetic radiation with that predicted by the Chapman solution. Results are presented in terms of the fraction of the atmosphere by mass penetrated by the energy deposited at the height of maximum energy deposition. Since the Chapman mechanism neglects subsequent scatterings, the altitudes of maximum energy depositions are higher than in our calculations. The effect is quite significant for the thin atmospheres with column densities $\lesssim 100 \text{ g cm}^{-2}$.

earlier, the primary contribution to the surface flux in thick atmospheres is the redistributed UV. Since the UV is primarily attenuated by molecular absorbers, atmospheres thick enough to deposit most of the incident energy above the absorbers will be indifferent to the angle of incidence of that radiation. Figure 10 illustrates the effect. In the thick atmospheres, we find that the angle of incidence has only a very small effect on the reemitted UV that reaches the surface in the biologically effective region of the spectrum; for thin atmospheres, the effect is negligible for both the incident radiation and the reemitted radiation because the optical depths are by definition small. We are therefore justified in neglecting the effects of the angle of incidence.

4. Relevance of results to astronomical sources

Our work is based on the fact that most planetary systems must be occasionally irradiated by bursts of X-ray and γ -ray photons from various astronomical events, a facet of planetary radiation environments that has been overlooked in the past. In order to place the above calculations in their proper context, we briefly summarize the major sources of such ionizing radiation, concentrating on the estimated frequencies and durations of the events.

4.1. Stellar flares

Surely the most frequent sources of stochastic irradiation by ionizing photons are flares from the parent star. For older solar-like stars the Sun provides the best-studied example. Solar flares are associated with ionizing radiation from keV X-rays to GeV γ -rays. The time variation of flare output depends on wavelength region and varies from flare to flare, e.g., Fig. 10.11 in Foukal (1990), Fig. 6.7 in Lang (2000), and Fig. 9.2 in Golub and Pasachoff (1997), with the gradually declining flare phase lasting up to an hour or more. The radiative energy release in a single flare varies by orders of magnitude, with the strongest solar flares ever observed emitting a few times 10^{32} erg (e.g., the 4 Nov 2003 flare). This corresponds to a flux above the Earth’s atmosphere of only $60 E_{32}$ $\text{erg cm}^{-2} \text{ s}^{-1}$, where E_{32} is the energy in units of 10^{32} erg and we adopted an average duration of 10 min. This is consistent with the maximum observed soft X-ray peak fluxes (Fig. 1 in Zirin et al. 2000).

Given the small historical interval over which such observations are available, even in the visual part of the spectrum, and the rapidly decreasing frequency of higher-energy events, it is reasonable to assume that still higher-energy events do occur, even if they have not been detected. The frequency distribution of flare energies from EUV to hard X-rays, derived from several space missions, can be described by a fairly robust power law (Crosby et al. 1998; Aschwanden et al. 2000; Lin et al. 2001; Güdel et al. 2003, and references therein), with log-log slope about -1.6 . Extrapolating these data to higher energies, we find that the frequency of flares of such large energy that 1% of the X-ray energy (using our result for an atmosphere of column density similar

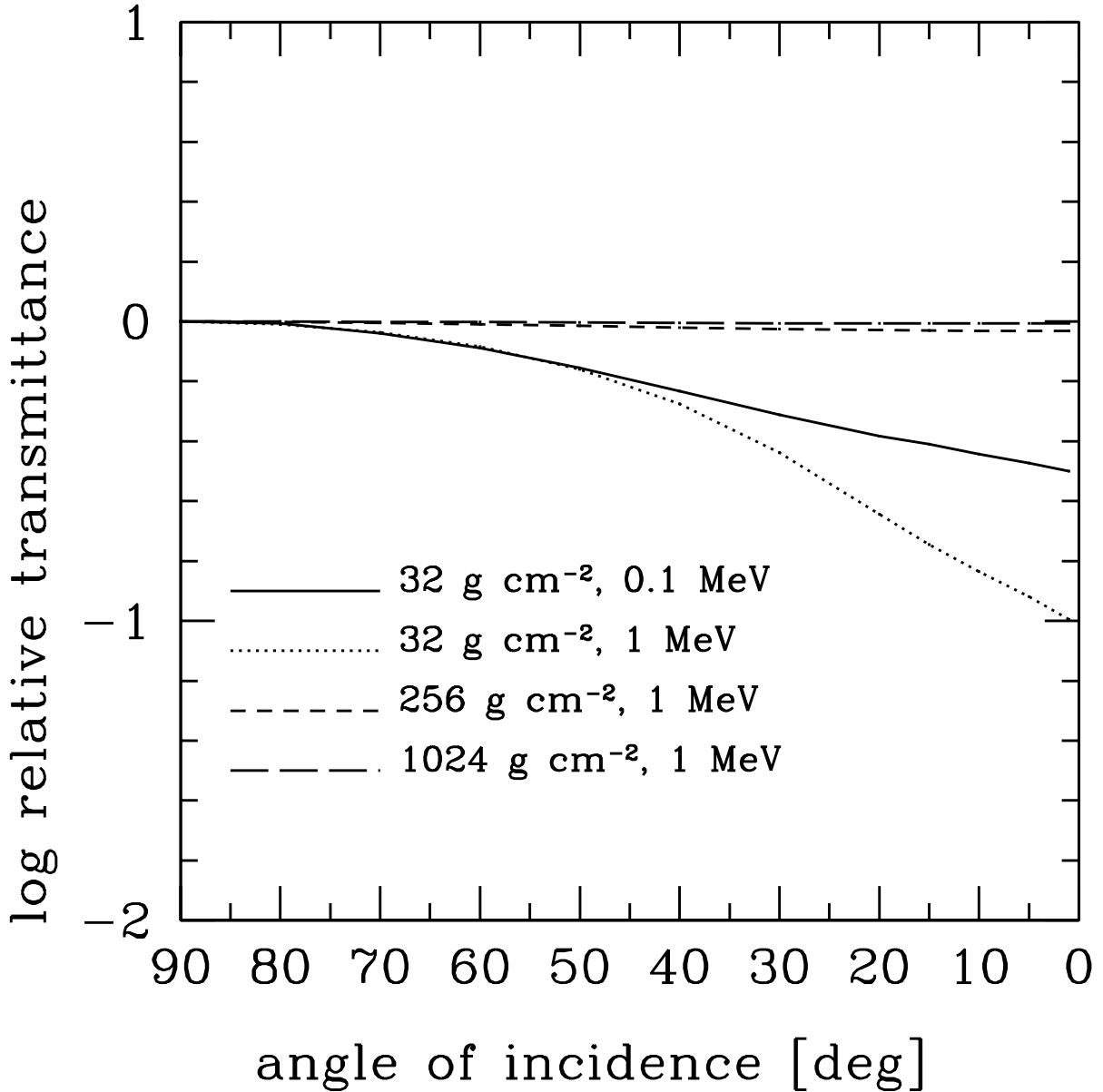


Fig. 10.— The effect of varying the angle of incidence. Plotted is the transmittance of the atmosphere as a function of angle of incidence relative to normal incidence. The curves include UV redistribution subjected to O_2/O_3 absorption in the transmittance (which raises the transmitted fractions above that of only the direct ionizing radiation). In the thick atmospheres, we find that the angle of incidence has only a very small effect on the reemitted UV that reaches the surface when redistribution is included; for thin atmospheres (and hence small optical depths), the effect is negligible for both the incident radiation and the redistributed radiation.

to the Earth’s) exceeds the solar UV flux at 1 AU of about 1×10^4 erg cm $^{-2}$ s $^{-1}$ at the Earth’s surface in the biologically active 200–320 nm region is about one per century. This frequency should be decreased if the steeper soft X-ray (0.1–0.8 nm) energy-frequency distribution recently found by Veronig et al. (2002) is correct.

That such flares do occur, even in old, weak-flaring stars like the Sun, is supported by Schaefer et al. (2000), who have identified nine cases of superflares with energy outputs of 10^{33} – 10^{38} erg on otherwise normal F8–G8 main sequence stars. These flares cannot be attributed to binaries, rapid rotation, or youth, and therefore may be common in solar-type stars. Schaefer et al. (2000) additionally estimate a very uncertain recurrence time of 10^2 – 10^3 yr.

Intense flares are much more frequent in younger solar-mass stars, as evidenced by both coronal X-ray emission of solar analogues of different ages (Guinan and Ribas 2002) and estimates of stellar wind momentum fluxes from solar-mass stars of different ages (Wood et al. 2002). It is also known that intense, although less frequent, flares occur in stars even more massive than the Sun, such as the F star EUV flares observed by Mullan and Mathioudakis (2000).

Using the available data on solar-mass stars of various ages, we find that the frequency of flares energetic enough to yield, after redistribution, UV fluxes in excess of the stellar flux should be on the order of once per 1–1000 yr depending on stellar age for habitable zone planets with atmospheres as thick as that of the Earth orbiting solar-mass and higher-mass stars. The frequency will be larger for planets with smaller atmospheric column densities; the dependence of the fraction of flux redistributed from X-rays to UV as a function of planetary atmosphere column density is shown in Fig. 7. Although even small changes in the UV irradiance can have sizeable effects on the Earth’s atmosphere (see Larkin et al. 2000), the brevity and large duty cycle of very energetic flares make their importance uncertain for solar-mass stars.

The situation is quite different for lower-mass, red main sequence stars of spectral type M. These stars are the most numerous stars in the Galaxy (see Chabrier 2003 and references therein), and calculations indicate that atmospheric circulation is sufficient for atmospheric retention and liquid water oceans in spite of synchronous rotation (Joshi et al. 1997; Joshi 2003). The potential importance of these stars for exobiology was first clearly recognized and discussed in detail by Heath et al. (1999).

Very low-mass stars spend a significant fraction of their long lives in a state dominated by strong and frequent flare activity (e.g., Shakhovskaya 1995). Such stars, called “flare stars,” “emission line stars,” or “UV Ceti stars” (after the prototype), are designated as spectral type dMe (see Gershberg et al. 1999 for an extensive database and bibliography).

These low mass stars are sources of frequent intense flares with energies as large as 10^{34} – 10^{35} erg in ionizing radiation (Cully et al. 1993; Hawley and Pettersen 1991) occurring roughly once per 100 hours of monitoring for some stars, with larger energies occurring at smaller rates. Figure 4 of Audard et al. (2000) shows that the rate of EUV flares with energies exceeding 10^{32} erg ranges from ~ 0.1 –100 per day, depending on the star’s coronal X-ray luminosity (which is correlated with

age). There are several examples of dMe stars with intense flares of energies exceeding 10^{34} erg in the blue and UV, as summarized by Liebert et al. (1999); see also Hawley and Pettersen (1991) and Pagano et al. (1997). Although these cases were not observed in the X-ray region, examples exist of comparable X-ray flares in other dMe stars (e.g., EV Lac, Favata et al. 2000). The larger and more frequent energy releases in very low mass star flares are accentuated by the proximity of conventional habitable zones: $\sim 0.05\text{--}0.15$ AU for stars in the range of masses $0.1\text{--}0.4 M_{\odot}$ (see Kasting et al. 1993). Since the habitable zone distance is partly determined by bolometric flux, habitable planets around these stars will be subjected to flare rates and fluxes many orders of magnitude larger than the Earth.

As a specific example, Cully et al. (1993) describe soft X-ray flares of energy above 10^{34} erg lasting over 2 hours for the dMe star AU Mic. This would give a flux above a habitable zone planet atmosphere of about 10^5 erg cm $^{-2}$ s $^{-1}$. Using the results of §3 for the UV redistribution, and the relative UV fluxes expected in dM stars, we find that the redistributed flare energy would swamp the stellar photospheric UV by an order of magnitude for a habitable planet atmosphere as thick as Earths. Considering the flare energy-frequency scaling for about 20 dMe stars in the U and B photometric bands by Gershberg and Shakhovskaya (1983) and more recent studies of harder radiation flares summarized by Güdel et al. (2003), we estimate that the UV radiation environment of very low-mass stars should be completely dominated by redistributed flare energy. The flares occur roughly once per day, with about an order of magnitude variation in this rate. Even the steady coronal X-ray emission may be important for the most active of these low-mass stars.

We expect biological activity and atmospheric chemistry to be strongly influenced by the exposure to such intensely fluctuating radiation environments, although the nature of the effects remains to be estimated. In particular, it is unknown whether such a mutationally rich environment would enhance or suppress the rate of evolution even in simple population genetics models.

4.2. Stellar explosions

Stellar explosions could also result in chemically and biologically significant fluxes and fluences of ionizing radiation, albeit with a much larger duty cycle than parent star flares. Supernovae produce γ -ray emission associated with the radioactive decay of freshly synthesized elements, mainly production of ^{56}Ni that decays to ^{56}Co and then to ^{56}Fe . Monte Carlo calculations of γ -ray deposition (e.g., Höflich et al. 1998) estimate a Type Ia supernovae release of 6×10^{48} erg per Type Ia event (see also Karam 2002); Type II supernovae are much less important. Using an average Galactic rate of Type Ia supernovae of 3×10^{-14} yr $^{-1}$ pc $^{-3}$ (Barbon et al. 1999), the average time between Type Ia supernovae at distance D_{kpc} kiloparsecs is found to be $T = 8 \times 10^3 D_{\text{kpc}}^{-3}$ yr. If 1% of the γ -rays are redistributed to UV by the mechanism discussed in the present work, we find that a biologically interesting fluence at the surface of a planet should occur once every 10^4 yr. However the associated flux would be swamped by the parent star UV flux for a habitable zone planet orbiting a solar-type parent star. The supernovae redistributed UV flux will only

exceed the parent star flux for low-mass host stars which have a smaller fraction of their flux in the UV, or for moons of giant planets at larger distances from solar-like host stars. We emphasize that the integrated mutation rate due to SN explosions is negligible compared to the background mutation rate because of the small durations compared to the recurrence timescale. Biologically, such intermittent hypermutation events may be most important for partial sterilization of planets and consequent effect on niche structure.

The γ -rays from supernovae can affect the atmospheric chemistry of habitable planets of solar-type stars, independently of any UV redistribution, through the direct effects of high-energy photons. The chemistry resulting from irradiation of a present-day Earth atmosphere was studied in detail by (Gehrels et al. 2003) using a single-scattering approximation for the radiative transfer. The more accurate transfer calculations in the present work agree fairly well with their results for energy deposition as a function of altitude in the thick-atmosphere, low-energy regime. However the expected rate of SN events near enough to significantly affect atmospheric chemistry is estimated to be only 1-2 per Gyr (Gehrels et al. 2003).

Supernova cosmic rays arriving later may be a more potent source of shower γ -rays and fast particles. From an evolutionary perspective, such events are especially interesting because diffusive propagation of cosmic rays implies long but uncertain exposure durations from 100 yr (Ruderman 1974) to 10^4 yr (Shklovsky 1969). The modulation of Galactic cosmic rays by the astrosphere as planetary systems pass through dense interstellar clouds (as suggested, for example, by Begelman and Rees 1976; Zank and Frisch 1999) may be more important than cosmic rays directly generated by the supernova itself. The statistics of fluctuations in astrospheric modulation of cosmic rays are modeled in detail in Smith and Scalo (2004).

Finally, we consider gamma-ray bursts as a potential source of intermittent ionizing radiation. Their energy output is so large that they could deliver a biologically important dose from essentially anywhere in the Galaxy, although the duration, ~ 10 sec on average, is so small that the main effects would be either partial sterilization of a planet or residual atmospheric chemistry perturbations. Recent evidence favors strong redshift evolution of the cosmic star-formation rate (e.g., Kewley et al. 2004 and references therein), which is needed to bring the observed gamma-ray burst rate to a Milky Way rate, so we use the “strong evolution” rates in Scalo and Wheeler (2002) to estimate the frequency of gamma-ray bursts at a given fluence. We find that the redistributed UV flux will only exceed the solar UV flux about once per 4×10^8 yr, with larger rates for lower-mass parent stars. For ozone depletion, the detailed study by Gehrels et al. (2003) of supernova direct gamma-ray irradiation requires an above-atmosphere fluence of $\sim 10^8$ erg cm $^{-3}$, giving a recurrence frequency of about 0.5 to 1 such events per Gyr, similar to but a little lower than was found by Gehrels et al. (2003) for SN γ -rays. The numbers are similar because the larger energies of gamma-ray bursts are offset by the smaller rates per unit volume compared to supernovae.

We conclude that the most important source of ionizing radiation for both biological and chemical effects are flares from parent stars, especially for low-mass stars. Supernovae and γ -ray bursts,

because of their large duty cycle, are probably only important if they induce partial extinction events, either directly through lethal dose exposure, or by atmospheric chemistry alterations (e.g., Melott et al. 2004). These events likely occur at a mean rate of one per 0.1 to 2 Gyr, depending on the mass of the parent star and the type of event involved. By contrast, the ionizing radiation environment of a habitable zone planet orbiting a low-mass star or a young solar-mass star probably involves a steady and frequent barrage of high-intensity flares with durations of minutes to hours occurring at rates of once per week to once per hour, depending on mass and age of parent star. The present work shows that a significant fraction of this radiation, rather than being absorbed high in the atmosphere, can reach the stratosphere or the surface in the form of redistributed UV radiation.

4.3. Energetic particles

Although we are only explicitly concerned with the effects of photons generated by astronomical events, high-energy particle emissions, mainly solar energetic particles (SEPs), solar chromospheric mass ejections (CMEs), and Galactic cosmic rays are also of interest, since their interaction with planetary atmospheres will result in the same kind of ultraviolet radiation through the generation of secondary electrons along the primary particle path. Some comparison of particles with photons is afforded by the recent summary of solar activity by Smith et al. (2003). Their Fig. 3 shows the flux of 1.8–3.8 MeV protons due to SEPs as a function of time during solar maximum and minimum. At solar maximum, the flux is of order $0.1 \text{ (cm}^2 \text{ s sr MeV)}^{-1}$, with excursions up to two orders of magnitude larger and smaller. Since it is the total energy flux that matters for redistribution to ultraviolet radiation, we convert this to a total energy flux at the mean SEP energy to obtain $1 \times 10^{-5} \text{ erg cm}^{-2} \text{ s}^{-1}$. Even allowing for a two order of magnitude enhancement, this flux is still small compared to a 10^{32} erg solar flare at 1 AU, which is $10 \text{ erg cm}^{-2} \text{ s}^{-1}$. The SEP flux is much more steady while the flare flux is only intermittent, so the fluence from SEPs is larger; however the redistributed UV flux from SEPs even at their peak is negligible. On the young Sun or on more active, lower-luminosity stars, the average flare energy and frequency is much larger, and one might expect the energetic particle flux to keep in step (e.g., Wood et al. 2002 on astrospheric momentum flux variations). We arrive at similar conclusions by examining the data for CME ~ 6 MeV protons from the 14 Jul 2000 Bastille day event (data from <http://soho.hascom.nasa.gov/hotshots> web site). The energy flux from Galactic cosmic rays is larger than that from solar cosmic rays, at least for older stars like our Sun (see Smith et al. 2003), and may vary considerably as the Sun travels through the Galaxy. Therefore we cannot rule out the importance of Galactic cosmic rays as a significant source of redistributed UV flux.

One type of solar particle that does seem important is the so-called “solar proton event,” a short-duration SEP burst of $\gtrsim 10$ MeV particles often associated with flares and presumably accelerated by coronal mass ejection shocks. The particle peak fluxes for the 35 most energetic of these events from 1973 to 2001 is given by El-Borie (2003). The average flux of particles with

energies above 30 MeV is $0.2 \text{ erg cm}^{-2} \text{ s}^{-1}$, while the largest is $1.6 \text{ erg cm}^{-2} \text{ s}^{-1}$. This is a lower limit because the proton spectrum rises with decreasing energy down to at least 10 MeV, so these events rival the most energetic solar flares in energy flux. In fact Shea and Smart (1996) list the strongest solar proton event recorded as having a number fluence of $3.4 \times 10^{10} \text{ cm}^{-2}$ at 1 AU. If the event lasted an hour (typical for SEP bursts), the energy release at the Sun would be 10 times that of the largest recorded solar flare.

For any energetic particle flux, whether Galactic or solar in origin, the resulting UV flux can be estimated by assuming most of the cosmic-ray energy is deposited in 35 eV secondary electrons that convert their kinetic energy into UV auroral radiation with the same efficiencies as found in the present paper for secondary electrons resulting from photon events.

5. Summary and Conclusions

The continuum UV emission from the Sun would have been very intense during the Archean era before the development of the ozone layer. Furthermore, the Sun was likely to have been much more active in the past when life first gained a foothold on Earth. Guinan and Ribas (2002) show that the coronal and X-ray to extreme UV emission of the young Sun were 100–1000 times stronger than those of the present Sun. Even now, solar flares are significant: they follow a power law fluence-per-interval relation that suggests that more powerful, but less frequent, flares are likely even for quiescent, aging solar type stars (Aschwanden et al. 2000). Mars may have once had a thick atmosphere that would still be subject to the strong redistribution of ionizing radiation into auroral UV in the manner we describe here, and it is now very susceptible to direct incident irradiation. Expanding our perspective to other stars hosting other planets, the case can easily be made that UV and ionizing radiation, including stochastic bursts of hard radiation, are the norm in our tumultuous Galaxy (Scalo et al. 2003).

To establish quantitatively the effects of ionizing radiation in terrestrial-like exoplanet atmospheres, we have used Monte Carlo models to propagate ionizing radiation through a suite of simple model atmospheres. We constrained the parameter space of the atmospheres by limiting the models to conditions that are consistent with “habitable” planets, in the sense that the atmosphere is thick enough to maintain liquid water on the surface, given enough ambient heating to keep the water in liquid form. We estimate the lower limit for atmospheric column depth for habitable planets to be about 30 g cm^{-2} . Above this limit, we characterize two types of atmospheres: “thin” and “thick.”

Our results can be summarized as follows.

1. Thin atmospheres with column density less than about 100 g cm^{-2} will directly transmit a substantial portion of any incident γ -ray flux. Even for these thin atmospheres, incident X-rays will be blocked because of the high cross section for photoabsorption. Contemporary Mars represents an example of this sort of thin atmosphere.

2. For planets with relatively thin atmospheres, the ionizing radiation spectrum at the surface from solar flares, supernovae, gamma-ray bursts or other sources of hard radiation should be relatively flat above 50–100 keV due to Comptonization, with a low-energy, photoabsorption cutoff.
3. We define thick atmospheres to be those with column density in excess of about 100 g cm^{-2} , in which both γ -rays and X-rays will be blocked. In this case, however, we show that, in the absence of UV blocking agents (O_3 or aerosols for instance), a substantial fraction of the incident energy will still arrive at the planetary surface as UV resulting from molecular excitation by secondary electrons produced by the Compton scattering of primary radiation and associated primary photoionization electrons. Typically 1–10% of the incident energy can reach the ground as this biologically-active “auroral” UV. This condition is typical of the Archean Earth where the only opacity to UV may be Rayleigh scattering.
4. A significant fraction of the incident energy may reach the surface even for contemporary Earth with its O_3 shield. We estimate that even today, a fraction of order 2×10^{-3} of incident hard flux will reach the surface of the Earth in the form of UV radiation in the 200–320 nm band, independent of the form of the incident ionizing radiation spectrum.
5. The spectrum of the redistributed UV radiation arriving at the planetary surface will depend on the rich and complex molecular emission line spectrum. We have considered relevant bands of N_2 to estimate that the net effect can be approximated by a continuous spectrum in which the energy flux is distributed approximately inversely with wavelength. We argue that essentially all molecules that might be substantially represented in the atmosphere of a habitable exoplanet would have electronic levels with similar spacings that would be excited with an efficiency comparable to N_2 .
6. We show that the results are not substantially affected by thermalization of the incident radiation since the ionized fractions of the atmosphere are typically low, nor by quenching, i.e., collisional deexcitation of the molecules, at the typical low electron densities, nor by the angle of incidence.
7. Our results show that low altitude “secondary ionospheres” can be produced in thick atmospheres if the ionizing radiation source is a supernova or gamma-ray burst. In the case of stellar flares, the existing ionospheres of thick atmospheres will be further ionized by a substantial margin. Ionization fractions in all cases of irradiation that exceed the parent star continuum are comparable to or greater than the steady-state terrestrial ionospheres. This phenomenon could affect atmospheric chemistry and global climate, especially in the case of the more frequent stellar flares on low-mass stars.
8. We do not know if early Mars had a thick atmosphere and, if so, whether or not it contained UV blocking agents (Haberle et al. 1994; Leblanc and Johnson 2001). The present work suggests that, even if it did, its early evolution, when life might have been forming or

expanding through evolutionary niches, would have been punctuated by bursts of reprocessed UV from stellar flares at relatively frequent intervals and again by more exotic but inevitable astronomical events at larger intervals.

Planets with thick atmospheres can be shielded from direct ionizing radiation and even from ordinary continuum UV if their atmospheres contain effective UV shields and still be subject to bursts of biologically significant UV. Smith et al. (2004) estimate that steady-state solar UV could be exceeded by redistributed UV from intense solar flares roughly once per decade. The redistributed flare energy rapidly increases in importance for the very common lower mass stars that have less continuum UV flux and more intense and frequent flares (see Güdel et al. 2003; Andreev et al. 2003).

The point of view that much of terrestrial and extraterrestrial life is driven by radiation sources was first outlined in the classic book by Shklovskii and Sagan (1966), but has lain substantially dormant since. Rothschild (1999) discusses a large number of possible relations between radiation and biological evolution. Significant aspects of evolution itself may be in response to changing radiation environments. Much DNA damage is either not repaired, leading to cell death, or is repaired precisely, in which case there is no mutation. In neither extreme is there evolution. On the contrary, a significant amount of current-day mutation is due to error-prone light-induced DNA damage repair of cyclobutane pyrimidine dimers incurred by UV radiation (e.g., Alpen 1998; Jagger 1985; von Sonntag 1987). In addition, the mechanisms involved in the repair of DNA damage due to UV and ionizing radiation are often the same as those involved in gene transfer and meiosis (Michod and Wojciechowski 1994 and references therein). It is conceivable that early life had to learn the techniques of radiation repair for survival, but then adapted them to powerful modes of evolution, first lateral gene transfer and then sexual reproduction. In this context of the possible fundamental importance of UV damage and repair, it is then especially interesting that planets with thick atmospheres that will shield surficial life from direct ionizing radiation will nevertheless shower the surface with UV irradiation in response to the stochastic astronomical radiation environment from the host star and more distant, yet significant Galactic events.

Acknowledgments

We thank Jim Kasting and Alex Pavlov for pointing out the two-stream solution for Rayleigh scattering, David Lambert for lending us nitrogen energy level data, Peter Höflich for first suggesting that the redistributed flux could be large, and two anonymous referees for comments and suggestions. DSS thanks the Harrington Doctoral Fellows Program and the NSF Graduate Research Fellowship Program for support. In addition, we gratefully acknowledge support from NSF grants AST 9907582 and AST 0098644.

A. Collisional Quenching

In our model, we assume all photon energy deposited in the atmosphere is reemitted as UV because of the efficiency of secondary electron excitation in a gas of very low ionization fraction. But in reality part of the reemission will be quenched by collisional deexcitation. Quenching was not included in our calculation because it would require solving the complete non-LTE level population rate equations for a variety of potential atmospheric constituents, a level of complexity and uncertainty beyond the scope of the present work. Nevertheless, we do wish to estimate its importance.

We first consider the usual two-level approximation. Rigorously, the two-level solution for the line intensity cannot be used because the principle of detailed balance between excitation and deexcitation rates does not hold when the secondary electrons have a non-Maxwellian velocity distribution. We instead require that all electron excitations result in an emitted line photon, except for the fraction suffering collisional deexcitation.

Ionization fractions are small enough in terrestrial-like exoplanet atmospheres that deexcitation occurs primarily via neutral atoms and molecules. The exception is the highest altitudes of atmospheres subjected to very high fluence ($\gtrsim 10^8$ erg cm $^{-2}$) stellar flares. We assume that the quenched transition is not forbidden, which would reduce the Einstein A_{ji} value by a large factor, as in terrestrial [OI] emission. The following method also applies (with some modification) for vibrational transitions within a given electronic level.

For the following estimate, we compute the excitation-deexcitation balance and obtain the relative importance of collisional quenching and radiative deexcitation in the most important N₂ auroral emission band systems listed in Table 1. The N₂⁺ level is important despite low ionization fractions because many of the secondary electrons will ionize N₂ to the B² Σ_u^+ excited state of N₂⁺, and subsequent fluorescence to the X² Σ_g^+ state yields the well-known strong 391.4 nm auroral band. The cross section for this process is large, and the efficiency of production of this band relative to all ionizations is about 6% (Banks and Kockarts 1973, p. 213). Following Jones (1974), we let dn_2/dt be the rate of excitation of the target molecule—N₂ in our case—to the upper electronic level by secondary electrons in the two-level scheme, A_{21} is the Einstein A value for the downward transition, Q_{21} is the thermally averaged collisional rate coefficient $\langle\sigma v\rangle$ for downward transitions due to collisions between the target and the dominant quenching particle M (N₂ and O₂ for the Earth), and n_2 and n_M are the number densities of the excited species and quenching species M, respectively. The balance between secondary electron excitation and the sum of radiative and collisional deexcitation can be written as

$$\frac{dn_2}{dt} = A_{21}n_2 + Q_{21}n_2n_M. \quad (\text{A1})$$

By dividing the balance equation by the unquenched rate $A_{21}n_2$, it is easy to show that the unquenched radiative deexcitation rate is reduced by a quenching factor f_Q :

$$f_Q = 1 + n_M Q_{21} / A_{21}. \quad (\text{A2})$$

We also define the critical density of quenching particles to be $n_{M,\text{crit}} \equiv A_{21}/Q_{21}$, at which the emission is halved.

We have estimated the critical quenching height z_Q in our models, at which $n_M(z_Q) = n_{M,\text{crit}}$, and the altitude of maximum energy deposition z_E , for two important UV transitions of N_2 . We can then gauge the amount by which a line is quenched by defining the quenching ratio, $\rho_Q \equiv z_Q/z_E$. When $\rho_Q \ll 1$, excitations take place where densities are low enough that collisional deexcitation is unimportant. The results of this approach can be applied to any other molecule of interest, depending on A_{ji} and Q_{ji} . Table 2 lists the relevant parameters for the N_2 band systems of Table 1 taken from Lofthus and Krupenie (1977), Huber and Herzberg (1979), and Banks and Kockarts (1973). Since the lifetimes of the upper molecular electronic states vary by orders of magnitude, we have chosen to illustrate the situation with two representative transitions of N_2 in Table 2—the Lyman-Birge-Hopfield and 2nd positive systems. These bands have A_{ji} values (10^4 and 10^8 , respectively) that cover the range of values for allowed transitions.

Figure 11 shows ρ_Q as a function of atmospheric column density for the two representative N_2 systems and two different incident photon energies. We can see from the plot that only Lyman-Birge-Hopfield (small A_{ji} value) is significantly quenched and only at very high incident energies, for which the altitude of maximum energy deposition z_E is very low. For X-ray incident energies, neither of the lines is significantly quenched, but the reemission in the L-B-H band would be reduced by a factor of about two. We can then conclude that reemission due to stellar flares incident on thin atmospheres are the least quenched, while the highest-energy irradiation by supernovae and gamma-ray burst γ -ray lines will be the most quenched.

The quenching effect as a function of incident energy is shown in Fig. 12. As expected the magnitude of quenching increases with increasing incident energy, since z_E decreases roughly logarithmically with optical depth. Again we see that the L-B-H system is quenched more than the 2nd positive transition, due to its lower A_{ji} . Interestingly, we see in both Figs. 11 and 12 that the incident energy sensitivity of ρ_Q is smaller for higher column density atmospheres. This behavior can be understood from the dependence of the quenching ration on the optical depth (which is proportional to the column density). Using the Chapman solution for the energy deposition, we

Band	A_{ji} [s $^{-1}$]	Q_{ji} [cm 3 s $^{-1}$]	$n_{M,\text{crit}}$ [cm $^{-3}$]
Vegard-Kaplan	0.53	1.5×10^{-11}	3×10^{10}
L-B-H	8.3×10^3	$\lesssim 3 \times 10^{-10}$	$\gtrsim 3 \times 10^{13}$
Herman-Kaplan	5.3×10^3	$\sim 10^{-10}$	$\sim 5 \times 10^{13}$
2nd positive	2.7×10^7	$\sim 10^{-10}$	$\sim 7 \times 10^{17}$
1st negative	1×10^7	4×10^{-10}	3×10^{16}

Table 2: Quenching factor data for N_2 UV band systems (Banks and Kockarts 1973; Lofthus and Krupenie 1977; Huber and Herzberg 1979). See Table 1 for definitions of the bands.

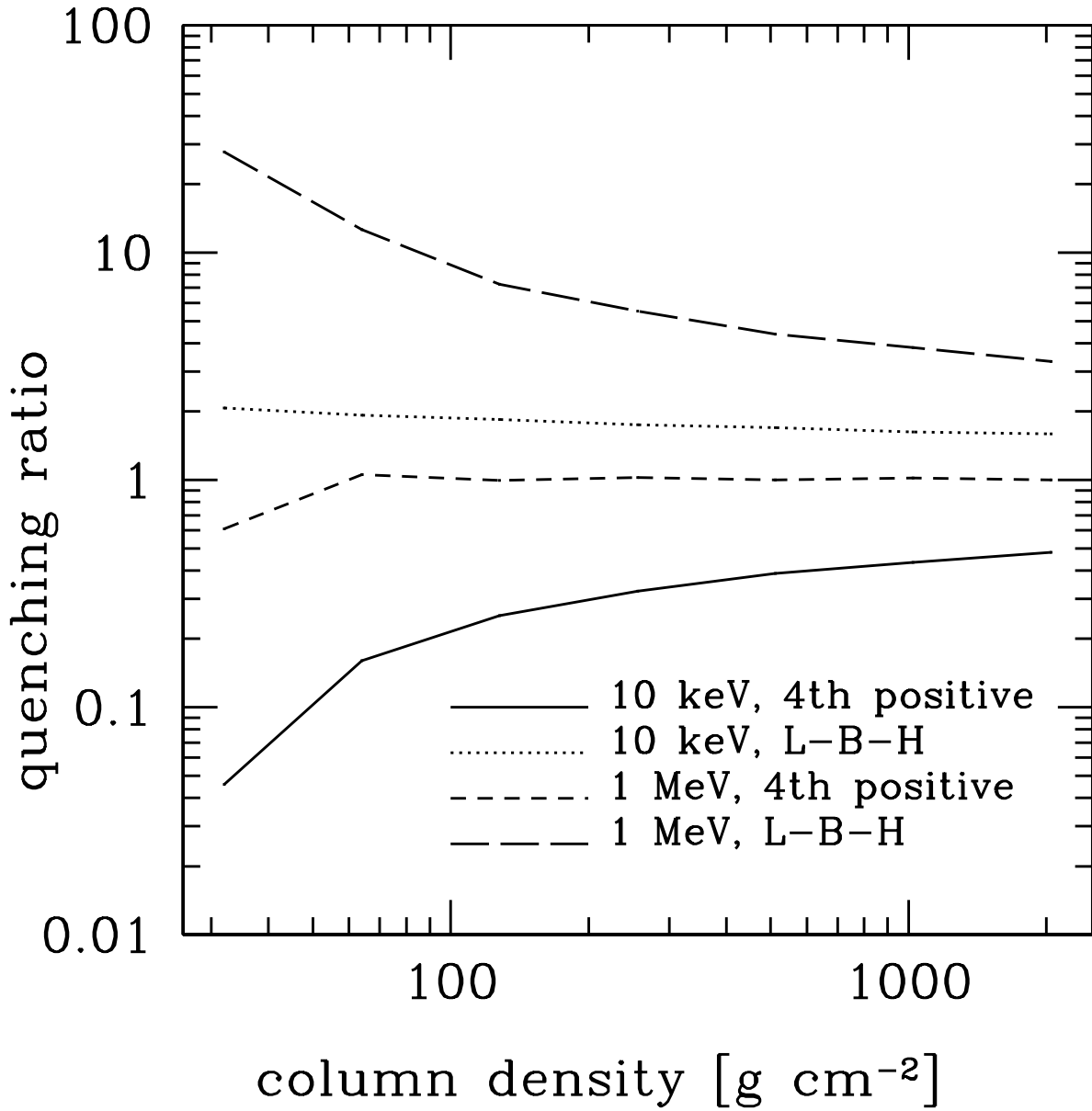


Fig. 11.— Quenching ratio ρ_Q as a function of column density for two representative molecular nitrogen systems. Only the Lyman-Birge-Hopfield system is significantly quenched and only at very high incident energies, for which the altitude of energy deposition z_E is very low. For hard X-ray incident energies, neither of the systems is completely quenched, but the reemission in the L-B-H band would be reduced by a factor of a few. The quenching ratio approaches unity for very thick atmospheres (see text for explanation).

can approximate the height of maximum as $z_{\max} = h \log \tau$ (see §3.4.1). We defined the altitude at which quenching becomes significant as z_Q such that $n(z_Q) = n_{\text{M,crit}}$. From this we have,

$$z_Q = -h \log(n_{\text{M,crit}}/n_0), \quad (\text{A3})$$

where n_0 is the number density of quenching molecules at the planet’s surface and h is the scale height. Taking the definition of the quenching ratio, we can write an approximation for it as

$$\begin{aligned} \rho_Q &= z_Q/z_E \\ &= -\frac{h \log(n_{\text{M,crit}}/n_0)}{h \log \tau} \\ &= \frac{\log(Q_{ji}\Sigma/A_{ji}h)}{\log(\Sigma\sigma)}, \end{aligned} \quad (\text{A4})$$

where Σ is the column density and σ is the cross section for energy deposition at the original incident energy. We can see from the form of this formula that the ratio $Q_{ji}\Sigma/A_{ji}h$ determines whether the quenching ratio is smaller or larger than 1, since all atmospheres of exoplanets considered habitable in this work have optical depths greater than unity at the incident energy. The only energy dependence enters in the denominator, in the optical depth τ . Rewriting,

$$\rho_Q = 1 + \frac{\log(Q_{ji}/A_{ji}\sigma h)}{\log \tau}. \quad (\text{A5})$$

Now we can see that as the column density (and hence τ) increases, the quenching ratio will approach unity. Furthermore, the quenching ratio increases as the incident energy increases because the dominant cross sections at keV to MeV energies (photoabsorption and Compton scattering) both decrease with higher energy. In other words, higher penetration of the atmosphere as the energy of the incident ionizing radiation increases reduces the UV reemission efficiency by depositing more of the energy in denser regions of the atmosphere.

Depending on the relative fluxes of the various auroral lines, the overall UV reemission will be quenched by a factor somewhere between the limits given in the plots. Since characteristic A_{ji} values and collisional deexcitation cross sections show a similar range for other molecules we can generalize our conclusions to the statement that quenching will only significantly affect the surficial fluences for transitions with A_{ji} values of $\lesssim 10^4 \text{ s}^{-1}$. Given that all of the lines listed in Table 1 are roughly equally strong, we expect that quenching will be insignificant for stellar flare irradiation, and for supernovae and gamma-ray bursts, the emission will likely be reduced by factor of only a few, depending on the A_{ji} value and column density.

B. Weighted Monte Carlo transport algorithm

An outline of the structure of the Monte Carlo code is as follows:

1. Initialize

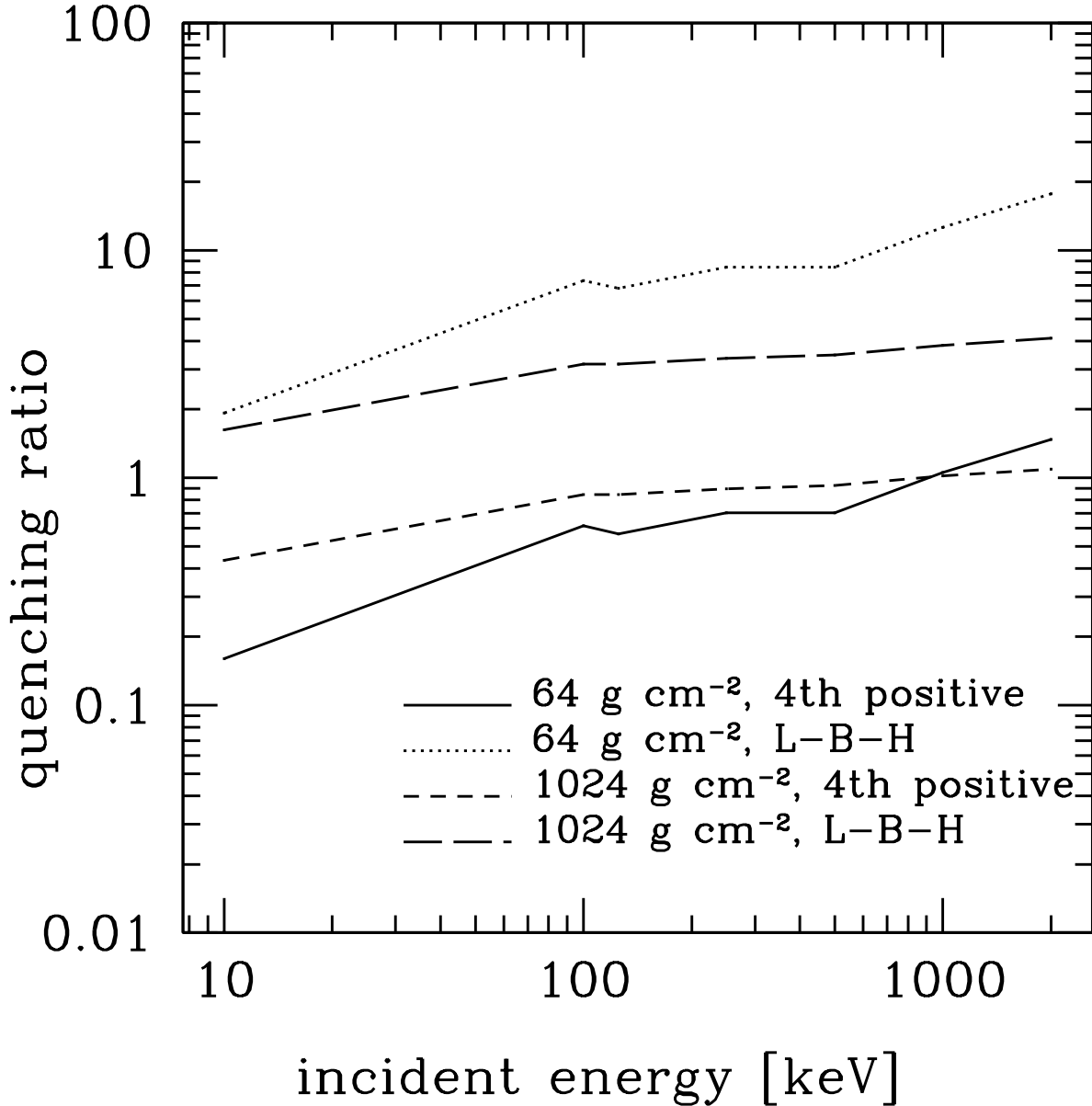


Fig. 12.— Quenching ratio ρ_Q as a function of incident energy for the two representative N_2 lines. Again we see that the L-B-H is quenched more than the 2nd positive transition, due to its lower A_{ji} . Interestingly, we again see that the difference in ρ_Q for the two lines is smaller for higher column densities, as can also be seen in Fig. 11 (see text for an explanation). Irregularities in the 64 g cm^{-2} curve are due to the smaller optical depth, i.e., fluctuations in the optical depth of the height of maximum energy deposition are magnified in altitude, leading to a larger uncertainty in z_E .

- (a) Assign each photon an initial incident energy E_0 drawn randomly from the specified incident spectrum.
- (b) Initialize the direction of propagation, θ_p . The angle of incidence, θ_i , is defined with respect to the plane of the atmosphere, but θ_p is oriented toward the ground. Hence for a normally incident ray $\theta_p = 0$ and $\theta_i = \pi/2$. We track the direction of propagation in three dimensions by a unit vector (v_x, v_y, v_z) that represents the direction of travel with respect to the ground, where the z-axis points downward to the ground. For the physics in this work, however, only the projection of the vector onto the z-axis (v_z) matters, where $v_z = \cos \theta_p$.
- (c) Set the statistical weight, w , of each photon to unity. Higher weights imply that the photon represents a packet of w photons, rather than one photon, which alters only normalizations.

2. Propagate

- (a) Recalculate the total cross sections for absorption and scattering.
- (b) For downward traveling photons, add a portion of the photon energy equal to $w \exp(-\tau/v_z)$ to the spectrum of flux received at the ground, where w is the current weight of that photon, τ is the optical depth from the photon's current altitude to the ground, and v_z is the downward component of the direction vector from above. This is the forced scattering procedure (cf. Witt 1977). This fraction of the weight removed represents the probability that the photon is still scattering (which we are forcing it to do) is simply one minus the probability that it did not scatter. If the photon is directed upward, the procedure is identical except the peeled-off weight is added to the spectrum of photons reflected by the planet and τ corresponds to the optical depth from the photon's altitude to the top of the atmosphere.
- (c) Sample a random optical depth to the interaction location from an exponential probability distribution $p(\tau) = \exp(-\tau)$ by generating a uniform deviate $R \in [0, 1]$ and inverting p to find the corresponding optical depth: $\tau = -\log R$. We choose an exponential distribution with unit mean because the photon behaves as part of a beam subjected to extinction and so has an intensity following Beer's Law, or $I(\tau) = I_0 \exp(-\tau)$. Thus the probability that a photon will traverse a distance corresponding to an optical depth τ unimpeded is $\exp(-\tau)$.
- (d) Move the photon a distance in the atmosphere corresponding to the randomly sampled optical depth. Since the atmosphere is based on an exponential density profile, the new altitude can be found analytically, eliminating one of the most computationally intensive procedures in Monte Carlo radiative transport—sampling a density field along a ray. From the sampled optical depth τ , we update the altitude z to z' according to

$$z' = -h \log \left[\exp \left(-\frac{z}{h} \right) + \frac{v_z \tau}{\chi h} \right], \quad (B1)$$

where χ is the total extinction coefficient, including Compton scattering and photoabsorption, and h is the scale height.

3. Interact

- (a) At the new location z' , multiply the statistical weight w by the scattering albedo a , which represents the probability that the photon still exists after the interaction. (If the photon were instead replaced by a continuous energy stream, a fraction a of the flux that interacted would be scattered, while a fraction $1 - a$ would be absorbed.)
- (b) Add the fraction of energy that was photoabsorbed to the spectrum of energy deposited at this layer. This represents the fraction of photons that would not have been scattered. Rather than absorbing all the energy of a fraction $1 - a$ of a packet of photons, the weighting technique stipulates instead to absorb that fraction of the energy of a single photon.
- (c) Choose a new propagation direction θ_p by sampling by a rejection technique from the differential Klein-Nishina formula, where the forward direction is parallel to (v_x, v_y, v_z) . The angular distribution is symmetric about this direction, so the angle about that axis is chosen from a uniform distribution. The sampled angle gives the direction change after the scattering event, so the a new direction vector must be calculated.
- (d) Update the photon energy based on the change in direction and the corresponding Compton energy loss. Add the Compton recoil electron energy to the spectrum of energy deposited in this layer. This energy is multiplied by the scattering albedo and the current photon weight in order to conserve energy.
- (e) Remove the current photon from the model if the updated weight is smaller than a pre-determined minimum value, since the photon is now statistically insignificant; otherwise, go to step 2 and repeat.

C. Code benchmarks

C.1. Pure scattering atmosphere

A standard solution to the radiative transfer equation can be obtained for pure scattering in the two-stream approximation. The approximation of pure scattering given by Schuster (1905) assumes (i) a plane-parallel atmosphere, (ii) a diffuse source incident at the top of the atmosphere, (iii) no sources inside the atmosphere, and (iv) a perfectly absorbing ground. With these conditions, the fraction of the incident flux transmitted through the atmosphere is $T \simeq 2/(2 + \tau/\mu)$, where τ/μ is the total optical thickness of the atmosphere divided by an angle cosine which represents the average angle of incidence of the radiation field. The actual value of μ can only be obtained by iteratively solving the radiation field until a value for μ converges; however as can be seen in our benchmarks, the approximation $\mu \simeq 1$ for normally incidence radiation is sufficiently accurate.

To compare our code, which includes more complicated physics than pure scattering, to a known scattering solution, we removed photoabsorption and altered the treatment of Compton scattering to make it conservative. Thus the photons were allowed to scatter with a cross section equal to the Compton cross section, but the energy changes were ignored. Figure 13 shows the comparison between the Monte Carlo code and the Schuster solution as a function of column density. The agreement is quite good for a Monte Carlo code, even for thick atmospheres, where the discrepancy is $\lesssim 15\%$. For reference, the μ required to bring the Schuster transmittance into agreement with ours is shown.

C.2. Beer-Lambert absorption

In the case of pure absorption, photons interact only once and then are removed from the model. To simplify the calculation, we treated the extinction coefficient as purely absorptive and removed all photons upon the first scattering. We found the agreement between the exponential attenuation approximation of the Beer’s law and the Monte Carlo code to be excellent. The Monte Carlo code shows an exponential dependence and matches Beer’s Law to better than 1 part in 10^4 for even the thickest atmospheres. This test is somewhat trivial, but disagreement would nevertheless indicate problems with the radiative transfer code.

C.3. Comptonization by cold electrons

A third test was performed to test solely the non-conservative, Compton scattering aspect of the code. We removed all photoelectric absorption and allowed each photon to Compton scatter a fixed number of times (100, in this case). In the limit of large scattering number, the Compton energy losses become small, and the photon energy spectrum approaches a Gaussian. Based on the results of Xu et al. (1991), we can write an analytic approximation for the spectrum as a function of initial energy and scattering number. The energy spectrum after the n -th scattering is given by Eq. 10 of Xu et al. (1991):

$$F_n(\lambda) = (2\pi\sigma_n^2)^{-1/2} \exp[-(\lambda - \lambda_n)^2/2\sigma_n^2], \quad (\text{C1})$$

where

$$\lambda_n = \lambda_{n-1} + 1 - \frac{4}{5\lambda_{n-1}} + O\left(\frac{1}{\lambda_{n-1}^2}\right), \quad (\text{C2})$$

$$\sigma_n^2 = \left(1 + \frac{8}{5\lambda_{n-1}^2}\right) \sigma_{n-1}^2 + \frac{2}{5} + O\left(\frac{1}{\lambda_{n-1}^2}\right), \quad (\text{C3})$$

and λ is in units of the Compton wavelength ($\lambda_c \equiv h/m_e c$).

Figure 14 shows a comparison of the Monte Carlo code and the Xu et al. formula for $n = 100$ scatterings of 2^{19} photons, each with an initial dimensionless wavelength (λ/λ_c) of 51.1 (equivalent

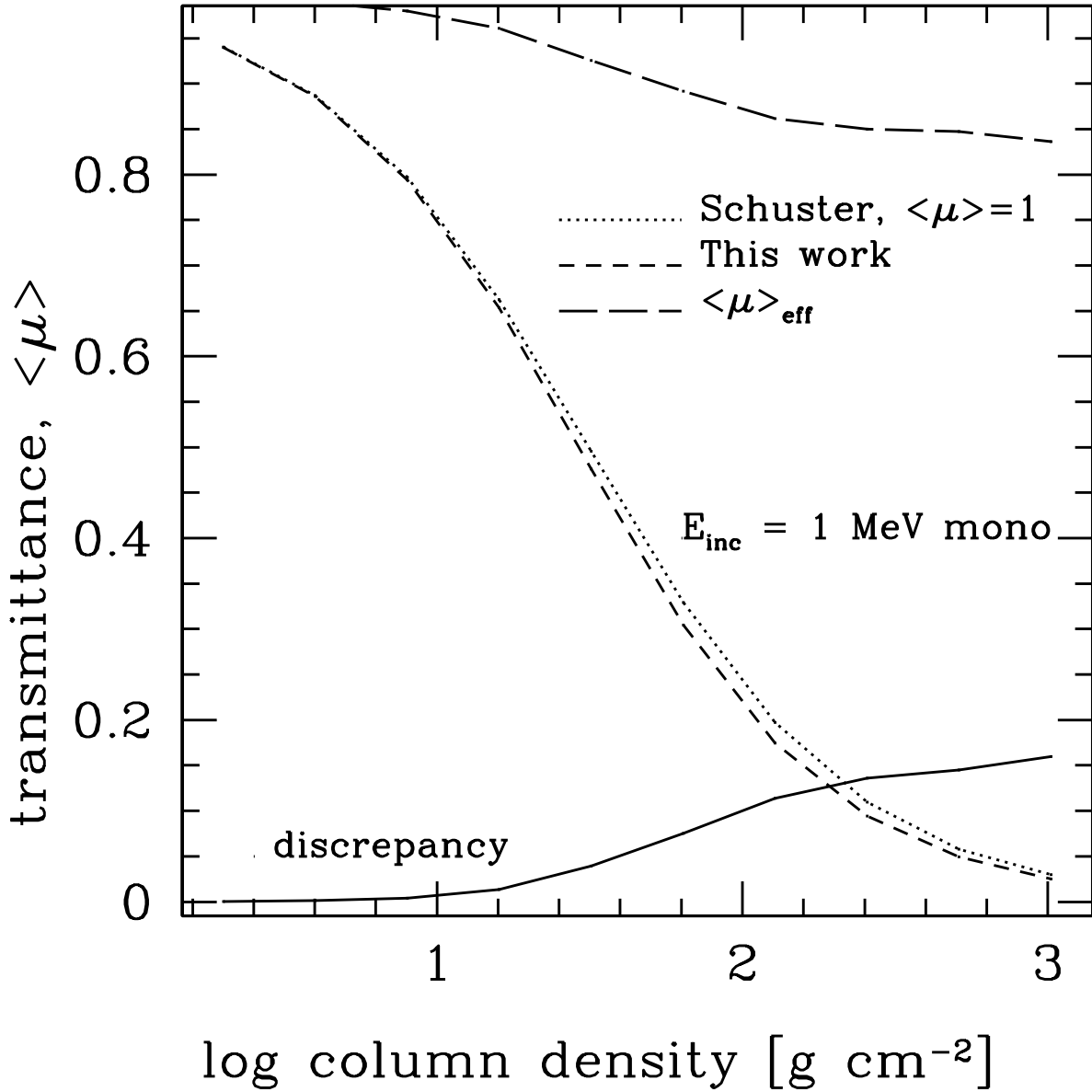


Fig. 13.— Comparison of the Monte Carlo code with the Schuster (1905) pure scattering solution. The agreement is quite good, even for thick atmospheres, where the radiation field deviates most from being monodirectional. The fractional discrepancy between the two results is due to the approximation of $\langle\mu\rangle = 1$ for the Schuster result, which would tend to overestimate the transmittance. The value of $\langle\mu\rangle_{\text{eff}}$ required to bring the Schuster data down to ours is shown and is $\gtrsim 0.8$ even for the thick atmospheres, implying that $\langle\mu\rangle \sim 1$ is an acceptable approximation. In our calculations, we assume normal incidence.

to an energy of 10 keV). The correspondence is excellent. The slight shift to longer wavelengths of the Monte Carlo results compared to the analytic approximation is due to the neglect of the higher order terms in the above formula for λ_n and σ_n^2 , which leads to an underestimation of the peak wavelength and variance when using the Xu et al. formula. The Monte Carlo code uses the full Compton energy shift formula and energy dependent cross section and thus should be more accurate.

D. Modification to the Schuster solution

Schuster (1905) solved the problem of a pure scattering atmosphere for a source above the atmosphere and a purely absorptive base (see §C.1). For the problem of the transmission of UV reemission in a planetary atmosphere, we adopt an average incidence angle cosine $\langle \mu \rangle = 0.5$, since our source of reemission is isotropic, and we expect the radiation field to be roughly so. Under these boundary conditions the fraction of the incident flux transmitted through the atmosphere is

$$T(\tau) = \frac{1}{1 + \tau}, \quad (\text{D1})$$

where τ is the total optical depth of the atmosphere. Similarly, the albedo of the atmosphere is $R \equiv 1 - T$, or

$$R(\tau) = \frac{\tau}{1 + \tau}. \quad (\text{D2})$$

For the UV redistribution in our work, we modified this solution to accurately handle reflection from the part of the atmosphere above each UV reemission layer, which was not present in the original Schuster solution. In our case, on a layer by layer basis, we have an isotropic source (a layer at which redistribution from ionizing to UV radiation occurs) sandwiched between two atmospheres with purely absorptive boundaries (both the ground and space do not reflect). The situation is illustrated in Fig. 15. We denote the optical depths of the upper and lower atmospheres as τ_{\uparrow} and τ_{\downarrow} , respectively. Since we are concerned with the amount of reemitted UV which reaches the surface, we set the transmission fraction of the “sandwich” to be the sum of the flux directly transmitted from the emission layer to the ground and the flux reflected between the two atmosphere layers and finally transmitted to the ground. Each atmosphere layer obeys the Schuster solution in isolation, but together the reflection terms increase the expected transmission by a significant margin. In a manner similar to the popular two-stream approximation, the isotropic source flux can be divided into a downward hemisphere ($\mu_+ \geq 0$) and an upward hemisphere ($\mu_- < 0$), each containing half of the total emitted flux. Starting with the downward hemisphere, the successive contributions to the surface flux from multiple reflections can be written easily. Starting with the flux transmitted without reflection, we add the contribution from the flux that has reflected once off the bottom atmospheric layer and then off the top atmospheric layer and is then transmitted through the bottom atmospheric layer. To that we add the flux that reflects off the bottom atmospheric layer, then the top, then the bottom, then the top, and then is transmitted through

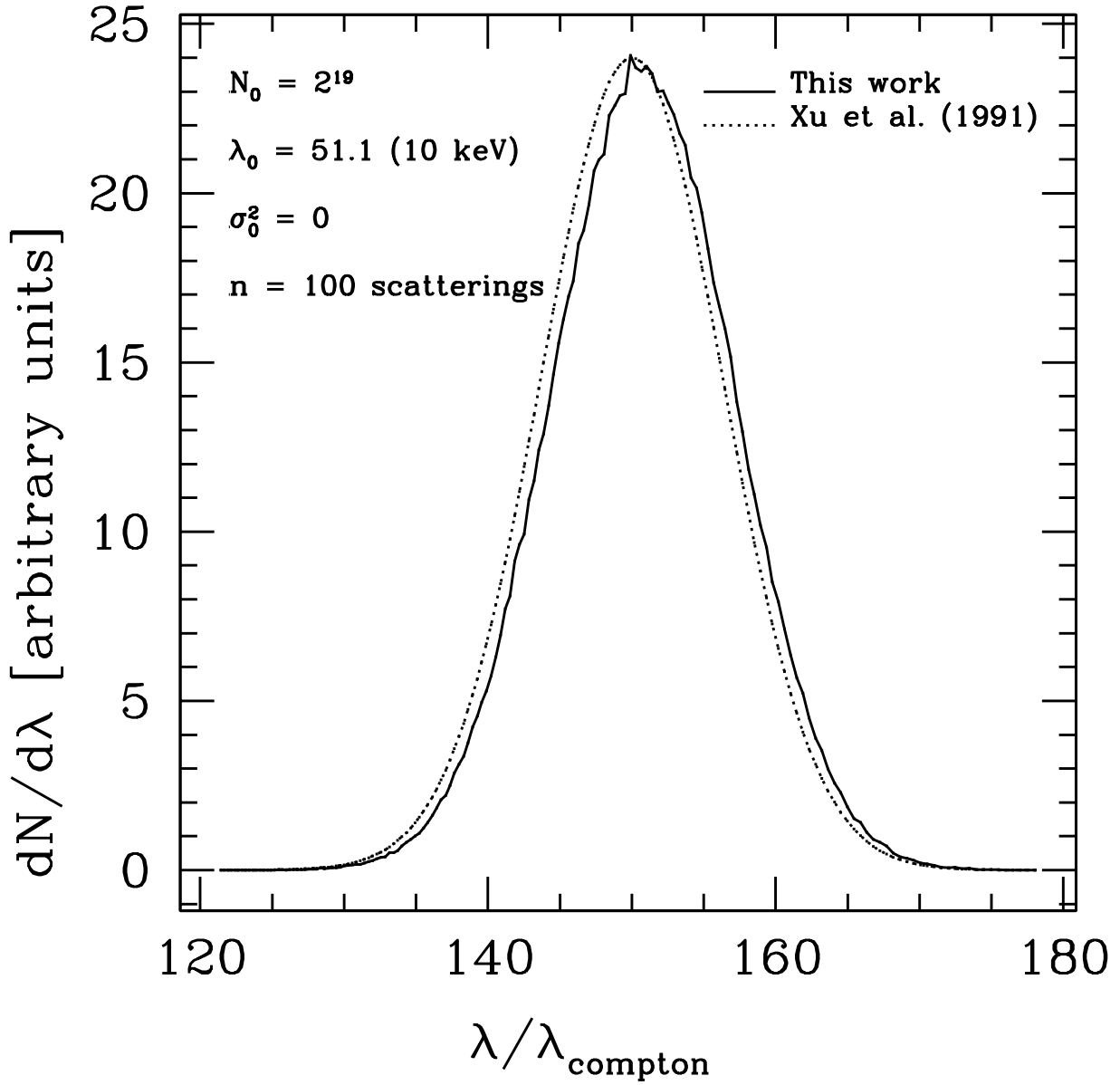


Fig. 14.— Comparison of the Monte Carlo code with the results of Xu et al. (1991). The slight shift to longer wavelengths of our code compared to the analytic approximation is due to the neglect of the higher order terms in the analytic expression for λ_n and σ_n^2 (see text), which leads to an underestimation of the peak wavelength and variance when using the Xu et al. formula (Eq. C1).

the bottom atmospheric layer, etc. Hence,

$$\begin{aligned}
 T(\mu_+) &= \frac{1}{1 + \tau_\downarrow} + \frac{\tau_\downarrow}{1 + \tau_\downarrow} \frac{\tau_\uparrow}{1 + \tau_\uparrow} \frac{1}{1 + \tau_\downarrow} \\
 &\quad + \left(\frac{\tau_\downarrow}{1 + \tau_\downarrow} \right)^2 \left(\frac{\tau_\uparrow}{1 + \tau_\uparrow} \right)^2 \frac{1}{1 + \tau_\downarrow} \\
 &\quad + \dots \\
 &= \frac{1}{1 + \tau_\downarrow} \sum_{p=0}^{\infty} \left[\frac{\tau_\downarrow \tau_\uparrow}{(1 + \tau_\downarrow)(1 + \tau_\uparrow)} \right]^p.
 \end{aligned} \tag{D3}$$

Since $\forall \tau_\downarrow, \tau_\uparrow > 0$, we have

$$\frac{\tau_\downarrow \tau_\uparrow}{(1 + \tau_\downarrow)(1 + \tau_\uparrow)} < 1, \tag{D4}$$

and we have a geometric series which can be summed to produce the transmission fraction for the downward hemisphere:

$$T(\mu_+) = \frac{1 + \tau_\uparrow}{1 + \tau_\uparrow + \tau_\downarrow}. \tag{D5}$$

A similar procedure for the upward hemisphere can be carried out, arriving at the above sum plus another factor of $R(\tau_\uparrow)$ accounting for the extra reflection from the upper atmosphere required to make the flux downward directed:

$$\begin{aligned}
 T(\mu_-) &= \frac{\tau_\uparrow}{1 + \tau_\uparrow} \frac{1}{1 + \tau_\downarrow} \\
 &\quad \times \sum_{p=0}^{\infty} \left[\frac{\tau_\downarrow \tau_\uparrow}{(1 + \tau_\downarrow)(1 + \tau_\uparrow)} \right]^p \\
 &= \frac{\tau_\uparrow}{1 + \tau_\uparrow + \tau_\downarrow}.
 \end{aligned} \tag{D6}$$

The total transmission of the source within the sandwich is

$$\begin{aligned}
 T &= \frac{1}{2} [T(\mu_+) + T(\mu_-)] \\
 &= \frac{1/2 + \tau_\uparrow}{1 + \tau_\uparrow + \tau_\downarrow}.
 \end{aligned} \tag{D7}$$

In the limit $\tau_\uparrow \gg \tau_\downarrow \gg 1$, we can see that $T \rightarrow 1$, which allows us to define $\tau_\uparrow \gg \tau_\downarrow$ as “close to the ground,” so no matter how optically thick the atmosphere, auroral emission “close to the ground” in a pure scattering atmosphere will reach the ground. The limit $\tau_\uparrow \ll \tau_\downarrow$ is the Schuster solution limit, in which $T \rightarrow 1/(2 + 2\tau_\downarrow)$. Note that this limit is actually half of the Schuster transmission because the source we consider is isotropic, while Schuster defines the entire source flux to be incident on the atmosphere.

REFERENCES

Adami, C., Ofria, C., Collier, T. C., 2000. Evolution of biological complexity. *Proc. Natl. Acad. Sci.* 97, 4463–4468.

Alpen, E. L., 1998. *Radiation Biophysics*. Academic Press, San Diego.

Andreevchev, A., Scalo, J., Smith, D. S., 2003. Very low-mass M stars as sites for habitability and evolution: The radiation environment. *Astrobiology*, submitted .

Aschwanden, M. J., Tarbell, T. D., Nightingale, R. W., Schrijver, C. J., Title, A., Kankelborg, C. C., Martens, P., Warren, H. P., Jun. 2000. Time variability of the “quiet” Sun observed with TRACE. II. Physical parameters, temperature evolution, and energetics of extreme-ultraviolet nanoflares. *Astrophys. J.* 535, 1047–1065.

Audard, M., Güdel, M., Drake, J. J., Kashyap, V. L., Sep. 2000. Extreme-ultraviolet flare activity in late-type stars. *Astrophys. J.* 541, 396–409.

Band, D., Matteson, J., Ford, L., Schaefer, B., Palmer, D., Teegarden, B., Cline, T., Briggs, M., Paciesas, W., Pendleton, G., Fishman, G., Kouveliotou, C., Meegan, C., Wilson, R., Lestrade, P., Aug. 1993. BATSE observations of gamma-ray burst spectra. I—Spectral diversity. *Astrophys. J.* 413, 281–292.

Banks, P. M., Kockarts, G., 1973. *Aeronomy: Part A*. Academic Press, NY.

Barbon, R., Buondi, V., Cappellaro, E., Turatto, M., 1999. The Asiago Supernova Catalogue—10 years after. *Astron. Astrophys. Supp.* 139, 531–536.

Begelman, M. C., Rees, M. J., May 1976. Can cosmic clouds cause climatic catastrophes. *Nature* 261, 298–299.

Brasseur, G. P., Orlando, J. J., Tyndall, G. S., 1999. *Atmospheric Chemistry and Global Change*. Oxford Univ. Press, NY.

Brown, R. T., 1973. Ionospheric effects of cosmic gamma-ray bursts. *Nature* 246, 83–84.

Cabrera-Juarez, E., Setlow, J. K., 1976. Mutation of *Haemophilus influenzae* transforming DNA *in vitro* with near-ultraviolet radiation: Action spectrum. *Mutation Res.* 35, 199–206.

Chabrier, G., 2003. Galactic stellar and substellar initial mass function. *Pub. Astron. Soc. Pac.* 115, 763–795.

Chamberlain, J., 1961. *Physics of Aurora and Airglow*. Acad. Press, NY.

Chamberlain, J. W., 1978. *Theory of planetary atmospheres: An introduction to their physics and chemistry*. Academic Press, NY.

Champion, K. S. W., Cole, A. E., Kantor, A. J., 1985. Standard and reference atmospheres. In: Jursa, A. S. (Ed.), *Handbook of Geophysics and the Space Environment*. Air Force Geophysics Lab, Springfield, VA.

Chapman, S., Jan. 1931. The absorption and dissociative or ionizing effect of monochromatic radiation in an atmosphere on a rotating Earth. *Proceedings of the Physical Society* 43, 26–45.

Chesson, P., Huntly, N., 1997. The roles of harsh and fluctuating conditions in the dynamics of ecological communities. *Amer. Natur.* 150, 519–553.

Cockell, C. S., 2002. Photobiological uncertainties in the Archaean and post-Archaean world. *Intl. J. Astrobiol.* 1, 31–38.

Crisp, D., 2000. Ionosphere. In: Cox, A. N. (Ed.), *Allen's Astrophysical Quantities*. Springer, NY, pp. 271–272.

Crosby, N., Vilmer, N., Lund, N., Sunyaev, R., Jun. 1998. Deka-keV X-ray observations of solar bursts with WATCH/GRANAT: Frequency distributions of burst parameters. *Astron. Astrophys.* 334, 299–313.

Crosby, N. B., Aschwanden, M. J., Dennis, B. R., Feb. 1993. Frequency distributions and correlations of solar X-ray flare parameters. *Solar Physics* 143, 275–299.

Cully, S. L., Siegmund, O. H. W., Vedder, P. W., Vallerga, J. V., Sep. 1993. Extreme Ultraviolet Explorer deep survey observations of a large flare on AU Microscopii. *Astrophys. J. Lett.* 414, L49–L52.

Edgar, B. C., Miles, W. T., Green, A. E. S., 1973. Energy deposition of protons in molecular nitrogen and applications to proton auroral phenomena. *J. Geophys. Res.* 78, 6595–6606.

El-Borie, M. A., 2003. Major solar-energetic particle fluxes: I. Comparison with the associated ground level enhancements of cosmic rays. *Astroparticle Phys.* 19, 549–558.

Evans, D., 1974. Precipitating electron fluxes formed by a magnetic field aligned potential difference. *J. Geophys. Res.* 79, 2853.

Fano, U., 1963. Penetration of protons, alpha particles, and mesons. *Ann. Rev. Nuclear Sci.* 13, 1–66.

Farquhar, J., Wing, B. A., McKeegan, K. D., Harris, J. W., Cartigny, P., Thiemens, M. H., 2002. Mass-independent sulfur of inclusions in diamond and sulfur recycling on early Earth. *Science* 298, 2369–2372.

Favata, F., Reale, F., Micela, G., Sciortino, S., Maggio, A., Matsumoto, H., 2000. An extreme X-ray flare observed on EV Lac by ASCA in July 1998. *Astron. Astrophys.* 353, 987–997.

Feder, M. E., Hofmann, G. E., 1999. Heat-shock proteins, molecular chaperones, and the stress response: Evolutionary and ecological physiology. *Ann. Rev. Physiol.* 61, 243–282.

Foukal, P., 1990. *Solar Astrophysics*. John Wiley & Sons, NY.

Fox, J. L., Victor, G. A., Apr. 1988. Electron energy deposition in N₂ gas. *Plan. Sp. Sci.* 36, 329–352.

Güdel, M., Audard, M., Kashyap, V. L., Drake, J. J., Guinan, E. F., Jan. 2003. Are coronae of magnetically active stars heated by flares? II. Extreme ultraviolet and X-ray flare statistics and the differential emission measure distribution. *Astrophys. J.* 582, 423–442.

Gehrels, N., et al., 2003. Ozone depletion from nearby supernovae. *Astrophys. J.* 585, 1169–1176.

Gershberg, R. E., Katsova, M. M., Lovkaya, M., Terebikh, A. V., Shakhovskaya, N. I., 1999. Catalogue and bibliography of the UV Ceti-type flare stars and related objects in the solar vicinity. *Astron. Astrophys. Suppl. Ser.* 139, 555–558.

Gershberg, R. E., Shakhovskaya, N. I., 1983. Characteristics of activity energetics of the UV Ceti-type flare stars. *Astrophys. Sp. Sci.* 95, 235–253.

Giraud, A., Matic, I., Tenaillon, O., Clara, A., Radman, M., Fons, M., Taddei, F., 2001. Costs and benefits of high mutation rates: Adaptive evolution of bacteria in the mouse gut. *Science* 291, 2606–2608.

Golub, L., Pasachoff, J. M., 1997. *The Solar Corona*. Cambridge Univ. Press, NY.

Gomez, F., Miikkulainen, R., 1997. Incremental evolution of complex general behavior. *Adaptive Behavior* 5, 317–342.

Gonzalez, G., Brownlee, D., Ward, P., Jul. 2001. The Galactic habitable zone: Galactic chemical evolution. *Icarus* 152, 185–200.

Gredel, R., Lepp, S., Dalgarno, A., Herbst, E., Dec. 1989. Cosmic-ray-induced photodissociation and photoionization rates of interstellar molecules. *Astrophys. J.* 347, 289–293.

Guinan, E. F., Ribas, I., 2002. Our changing Sun: The role of solar nuclear evolution and magnetic activity on Earth's atmosphere and climate. In: Montesinos, B., Gimenez, A., Guinan, E. F. (Eds.), *The Evolving Sun and its Influence on Planetary Environments*. Vol. 269. Astro. Soc. Pac., San Francisco, pp. 85–106.

Haberle, R. M., Tyler, D., McKay, C. P., Davis, W. L., May 1994. A model for the evolution of CO₂ on Mars. *Icarus* 109, 102–120.

Hammersley, J. M., Handscomb, D. C., 1979. *Monte Carlo Methods*. Chapman and Hall, London.

Hawley, S. L., Pettersen, B. R., 1991. The great flare of 1985 April 12 on AD Leonis. *Astrophys. J.* 378, 725–741.

Heath, M. J., Doyle, L. R., Joshi, M. M., Haberle, R. M., 1999. Habitability of planets around red dwarf stars. *Origins Life Evol. Biosphere* 29, 405–424.

Henke, B. L., Gullikson, E. M., Davis, J. C., 1993. X-ray interactions: Photoabsorption, scattering, transmission, and reflection at $E = 50\text{--}30,000$ eV, $Z = 1\text{--}92$. *Atomic Data and Nuclear Data Tables* 54, 181.

Höflich, P., Wheeler, J. C., Khokhlov, A., Jan. 1998. Hard X-rays and gamma rays from type Ia supernovae. *Astrophys. J.* 492, 228–245.

Huber, K. P., Herzberg, G., 1979. *Molecular Spectra and Molecular Structure. IV. Constants of Diatomic Molecules*. van Nostrand Reinhold, NY.

Ingersoll, A. P., Nov. 1969. The Runaway Greenhouse: A History of Water on Venus. *J. of Atmos. Sci.* 26, 1191–1198.

Itoh, T., Martin, W., Nei, M., 2002. Acceleration of genomic evolution caused by enhanced mutation rate in endocellular symbionts. *Proc. Natl. Acad. Sci.* 99, 12944–12948.

Jagger, J., 1985. Solar-UV actions on living cells. Prager Publ., NY.

Jones, A. V. J., 1974. *Aurora*. Reidel, Dordrecht.

Joshi, M., 2003. Climate Model Studies of Synchronously Rotating Planets. *Astrobiology* 3, 415–428.

Joshi, M. M., Haberle, R. M., Reynolds, R. T., Oct. 1997. Simulations of the atmospheres of synchronously rotating terrestrial planets orbiting M dwarfs: Conditions for atmospheric collapse and the implications for habitability. *Icarus* 129, 450–465.

Kallman, T. R., McCray, R., Dec. 1982. X-ray nebular models. *Astrophys. J. Supp.* 50, 263–317.

Kalos, M. H., Whitlock, P. A., 1986. *Monte Carlo Methods, Vol. I: Basics*. Wiley, NY.

Karam, P. A., 2002. Gamma and neutrino radiation dose from gamma ray bursts and nearby supernovae. *Health Physics* 82, 491.

Kasting, J. F., Jun. 1988. Runaway and moist greenhouse atmospheres and the evolution of earth and Venus. *Icarus* 74, 472–494.

Kasting, J. F., Donahue, T. M., 1980. The evolution of atmospheric ozone. *J. Geophys. Res.* 85, 3255–3263.

Kasting, J. F., Holland, H. D., Pinto, J. P., Oct. 1985. Oxidant abundances in rainwater and the evolution of atmospheric oxygen. *J. Geophys. Res.* 90, 10497.

Kasting, J. F., Whitmire, D. P., Reynolds, R. T., Jan. 1993. Habitable zones around main sequence stars. *Icarus* 101, 108–128.

Kasturirangan, K., Rao, U. R., Rastogi, R. G., Chakravarty, S. C., Sharma, D. P., Jun. 1976. Ionospheric effects of transient celestial X-ray and gamma-ray events. *Astrophys. and Sp. Sci.* 42, 57–62.

Kewley, L. J., Geller, M. J., Jansen, R. A., 2004. [OII] as a star formation rate indicator. *Astron. J.* 128, 1263–1274.

Krucker, S., Lin, R. P., 2002. Relative timing and spectra of solar flare hard X-ray sources. *Solar Phys.* 210, 220–243.

Lang, K. R., 2000. *The Sun from Space*. Springer-Verlag, NY.

Larkin, A., Haigh, J. D., Djavidnia, S., 2000. The effect of solar UV irradiance variations on the Earth's atmosphere. *Sp. Sci. Rev.* 94, 199–214.

Leblanc, F., Johnson, R. E., May 2001. Sputtering of the Martian atmosphere by solar wind pick-up ions. *Plan. Sp. Sci.* 49, 645–656.

Levy, M., Miller, S. L., 1998. The stability of the RNA bases: Implications for the origin of life. *Proc. Natl. Acad. Sci.* 95, 7933–7938.

Liebert, J., Kirkpatrick, J. D., Reid, I. N., Fisher, M. D., 1999. A 2MASS ultracool M dwarf observed in a spectacular flare. *Astrophys. J.* 519, 345–353.

Lin, R. P., Feffer, P. T., Schwartz, R. A., 2001. Solar hard X-ray bursts and electron acceleration down to 8 keV. *Astrophys. J. Lett.* 557, L125–128.

Lingenfelter, R. E., Rothschild, R. E., 2000. Gamma-ray and neutrino astronomy. In: Cox, A. N. (Ed.), *Allen's Astrophysical Quantities*. Springer, NY, pp. 215–234.

Lofthus, A., Krupenie, P. H., 1977. The spectrum of molecular nitrogen. *J. Phys. Chem. Ref. Data* 6, 113–307.

Matsumoto, M., Nishimura, T., 1998. A 623-dimensionally equidistributed uniform pseudorandom number generator. *ACM Trans. on Modeling and Computer Simulation* 8, 3–27.

Melott, A. L., Lieberman, B. S., Laird, C. M., Martin, L. D., Medvedev, M. V., Thomas, B. C., Cannizzo, J. K., Gehrels, N., Jackman, C. H., 2004. Did a gamma-ray burst initiate the late Ordovician mass extinction? *Intl. J. Astrobiol.* in press.

Michod, R. E., Wojciechowski, M. F., 1994. DNA repair and the evolution of transformation in the bacterium *Bacillus subtilis*. IV. DNA damage increases transformation. *J. Evol. Bio.* 7, 147–175.

Mitchner, M., Kruger, C. H., 1973. *Partially Ionized Gases*. John Wiley & Sons, NY.

Molina-Cuberos, G. J., Stumptner, W., Lammer, H., Komle, N. I., 2001. Cosmic ray and UV radiation models on the ancient Martian surface. *Icarus* 154, 216–222.

Moriarty, D. E., Miikkulainen, R., 1995. Discovering complex Othello strategies through evolutionary neural networks. *Conn. Sci.* 7, 195–209.

Moriarty, D. E., Miikkulainen, R., 1999. Learning sequential decision tasks through symbiotic evolution of neural networks. In: Honavar, V., Patel, M., Balakrishnan, K. (Eds.), *Advances in the Evolutionary Synthesis of Neural Systems*. MIT Press, Cambridge, pp. 367–382.

Moxon, E. R., Rainey, P. B., Nowak, M. A., Lenski, R. E., 1994. Adaptive evolution of highly mutable loci in pathogenic bacteria. *Curr. Biol.* 4, 23–33.

Mullan, D. J., Mathioudakis, M., 2000. Extreme-ultraviolet flares in an F2 star. *Astrophys. J.* 544, 475–480.

Nilsson, A., 1996. *Ultraviolet Reflections: Life under a Thinning Ozone Layer*. Wiley & Sons, NY.

Omongan, E., Baird, G. A., Jun. 1976. Ionospheric techniques for the detection of transient X- and gamma-ray bursts. *Astrophys. and Sp. Sci.* 42, 63–67.

Pagano, I., Ventura, R., Rodono, M., Peres, G., Micela, G., 1997. A major optical flare on the recently discovered X-ray active dMe star G 102-21. *Astron. Astrophys.* 318, 467–471.

Paul, N. D., Gwynn-Jones, D., 2003. Ecological roles of solar UV radiation: Towards an integrated approach. *Trends Ecology Evol.* 18, 48–55.

Peak, I. R. A., Jennings, M. P., Hood, D. W., Bisercic, M., Moxon, E. R., 1996. Tetrameric reeat units associated with virulence factor phase variation in *Haemophilus* also occur in *Neisseria* spp. and *Moraxella catarrhalis*. *FEMS Microbiol. Lett.* 137, 109.

Peterson, W. K., Beaty, E. C., Opal, C. B., 1972. Measurements of energy and angular distributions of secondary electrons produced in electron-impact ionization of helium. *Phys. Rev. A* 5, 712–723.

Peterson, W. K., Opal, C. B., Beaty, E. C., 1971. Energy distributions of electrons ejected in ionizing collisions of electrons with helium. *J. Physics B* 4, 1020–1025.

Pinaud, R., Tremere, L. A., Penner, M. R., Hess, F. F., Robertson, H. A., Currie, R. W., 2002. Complexity of sensory environment drives the expression of candidate-plasticity gene, nerve growth factor induced-A. *Neuroscience* 112, 573–582.

Prasad, S. S., Tarafdar, S. P., Apr. 1983. UV radiation field inside dense clouds—its possible existence and chemical implications. *Astrophys. J.* 267, 603–609.

Preece, R. D., Briggs, M. S., Mallozzi, R. S., Pendleton, G. N., Paciesas, W. S., Band, D. L., Jan. 2000. The BATSE gamma-ray burst spectral catalog. I. High time resolution spectroscopy of bright bursts using high energy resolution data. *Astrophys. J. Supp.* 126, 19–36.

Pugliucci, M., 2002. Buffer zone. *Nature* 417, 598.

Radman, M., Matic, I., Taddei, F., 1999. Evolution of evolvability. *Ann. NY Acad. Sci* 870, 146–155.

Radman, M., Taddei, F., Matic, I., 2000. Evolution-driving genes. *Res. Microbiol.* 151, 91–95.

Rainey, P. B., Travisano, M., 1998. Adaptive radiation in a heterogeneous environment. *Nature* 394, 69–72.

Reznick, D. N., Shaw, F. H., Rodd, F. H., Shaw, R. G., 1997. Evaluation of the rate of evolution in natural populations of guppies (*Poecilia reticulata*). *Science* 275, 1934–1937.

Ross, R. R., Oct. 1979. Spectral formation in compact X-ray sources. *Astrophys. J.* 233, 334–343.

Ross, R. R., Fabian, A. C., Mar. 1993. The effects of photoionization on X-ray reflection spectra in active galactic nuclei. *Mon. Not. Royal. Astron. Soc.* 261, 74–82.

Rothschild, L. J., 1999. Enigmatic microorganisms and life in extreme environments. In: Seckbach, J. (Ed.), *Microbes and Radiation*. Kluwer, Dordrecht, pp. 551–562.

Ruderman, M. A., 1974. Possible consequences of nearby supernova explosions for atmospheric ozone and terrestrial life. *Science* 184, 1079–1081.

Rutherford, S. L., Lindquist, S., 1998. Hsp90 as a capacitor for morphological evolution. *Nature* 396, 336–342.

Sagan, C., Chyba, C., 1997. The early faint Sun paradox: Organic shielding of ultraviolet-labile greenhouse gases. *Science* 276, 1217–1221.

Scalo, J., Wheeler, J. C., Feb. 2002. Astrophysical and astrobiological implications of gamma-ray burst properties. *Astrophys. J.* 566, 723–737.

Scalo, J., Wheeler, J. C., Williams, P., 2003. Intermittent jolts of galactic UV radiation: mutagenetic effects. In: Celnikier, L. M. (Ed.), *Frontiers of Life*. Vol. astro-ph/0104209, in press.

Schaefer, B. E., King, J. R., Deliyannis, C. P., Feb. 2000. Superflares on ordinary solar-type stars. *Astrophys. J.* 529, 1026–1030.

Schuster, A., Jan. 1905. Radiation through a foggy atmosphere. *Astrophys. J.* 21, 1–22.

Seager, S., Sasselov, D. D., Aug. 1998. Extrasolar giant planets under strong stellar irradiation. *Astrophys. J. Lett.* 502, L157–L161.

Setlow, R. B., Pollard, E. C., 1962. *Molecular Biophysics*. Addison-Wesley, Reading, MA.

Shakhovskaya, N. I., 1995. Flare activity among nearby stars. In: Greiner, J., Duerbeck, H. W., Gershberg, R. E. (Eds.), *Flares and Flashes: Proc. IAU Colloq. Vol. 151*. Springer, NY, pp. 61–62.

Shea, M. A., Smart, D. F., 1996. Solar proton fluxes as a function of the observation location with respect to the parent solar activity. *Adv. Space Res.* 17, 225–228.

Shklovskii, I. S., Sagan, C., 1966. *Intelligent Life in the Universe*. Holden-Day, San Francisco.

Shklovsky, I. S., 1969. *Supernovae*. John Wiley & Sons. Ltd, NY.

Smith, D. S., Scalo, J., 2004. Statistics of galactic cosmic-ray modulation variations on habitable planets. *Astrophys. J.*, in preparation .

Smith, D. S., Scalo, J., Wheeler, J. C., 2004. Importance of biologically active aurora-like UV emission: Stochastic irradiation of Earth and Mars. *Origins of Life and Evolution of the Biosphere*, in press .

Smith, E. J., Marsden, R. G., Balogh, A., Gloeckler, G., Geiss, J., McComas, D. J., McKibben, R. B., MacDowall, R. J., Lanzerotti, L. J., Krupp, N., Krueger, H., Landgraf, M., 2003. The Sun and heliosphere at solar maximum. *Science* 302, 1165–1169.

Sniegowski, P. D., Gerrish, P. J., Johnson, T., Shaver, A., 2000. The evolution of mutation rates: Separating causes from consequences. *BioEssays* 22, 1057–1066.

Spitzer, L., 1962. *Physics of Fully Ionized Gases*. Wiley-Interscience, NY.

Spitzer, L., 1978. Physical processes in the interstellar medium. Wiley-Interscience, NY.

Swartz, W., Nisbet, J., Green, A., 1971. Analytic expression for the energy-transfer rate from photoelectrons to thermal-electrons. *J. Geophys. Res.* 76, 8425.

Tavani, M., Band, D., Ghirlanda, G., 2000. Time Resolved GRB Spectroscopy. In: Kippen, R. M., Mallozzi, R. S., Fishman, G. J. (Eds.), *AIP Conf. Proc. 526: Gamma-ray Bursts, 5th Huntsville Symposium*. pp. 185–189.

Tucker, W. H., Koren, M., Sep. 1971. Radiation from a high-temperature low-density plasma: The X-ray spectrum of the solar corona. *Astrophys. J.* 168, 283–312.

Turnbull, M. C., Tarter, J. C., Mar. 2003. Target selection for SETI. I. A catalog of nearby habitable stellar systems. *Astrophys. J. Supp.* 145, 181–198.

van Belkum, A., Scherer, S., van Alphen, L., Verbrugh, H., 1998. Short-sequence DNA repeats in prokaryotic genomes. *Microbiol. Mol. Biol. Rev.* 62, 275.

Veronig, A., Temmer, M., Hanslmeier, A., Otruba, W., Messerotti, M., 2002. Temporal aspects and frequency distributions of solar soft X-ray flares. *Astron. Astrophys.* 382, 1010–1080.

von Sonntag, C., 1987. The chemical basis of radiation biology. Taylor & Francis, NY.

Ward, P. D., Brownlee, D., 2000. Rare Earth: Why Complex Life is Uncommon in the Universe. Copernicus Books, NY.

Watson, A. M., Henney, W. J., Oct. 2001. An efficient Monte Carlo algorithm for a restricted class of scattering problems in radiation transfer. *Revista Mexicana de Astronomia y Astrofisica* 37, 221–236.

Whalen, J. A., O’Neil, R. R., Picard, R. H., 1985. The aurora. In: Jursa, A. S. (Ed.), *Handbook of Geophysics and the Space Environment*. pp. 12–1.

Wiechert, U. H., 2002. Earth’s early atmosphere. *Science* 298, 2341–2342.

Witt, A. N., Sep. 1977. Multiple scattering in reflection nebulae. I—A Monte Carlo approach. *Astrophys. J. Supp.* 35, 1–6.

Wood, B. E., Muller, H. R., Zank, G. P., Linsky, J. L., 2002. Measured mass-loss rates of solar-like stars as a function of age and activity. *Astrophys. J.* 574, 412–425.

Xu, Y., Ross, R. R., McCray, R., Apr. 1991. Comptonization of gamma rays by cold electrons. *Astrophys. J.* 371, 280–288.

Yung, Y. L., DeMore, W. B., 1999. Photochemistry of planetary atmospheres. Oxford Univ. Press, NY.

Zank, G. P., Frisch, P. C., 1999. Consequences of a change in the Galactic environment of the Sun. *Astrophys. J.* 518, 963–965.

Zirin, H., Sammis, I., Tang, F., 2000. The magnetic circumstances of large flares. In: Ramaty, R., Mandzhavidze, N. (Eds.), *ASP Conf. Ser.* 206: High Energy Solar Physics Workshop—Anticipating HESSI. pp. 37–42.

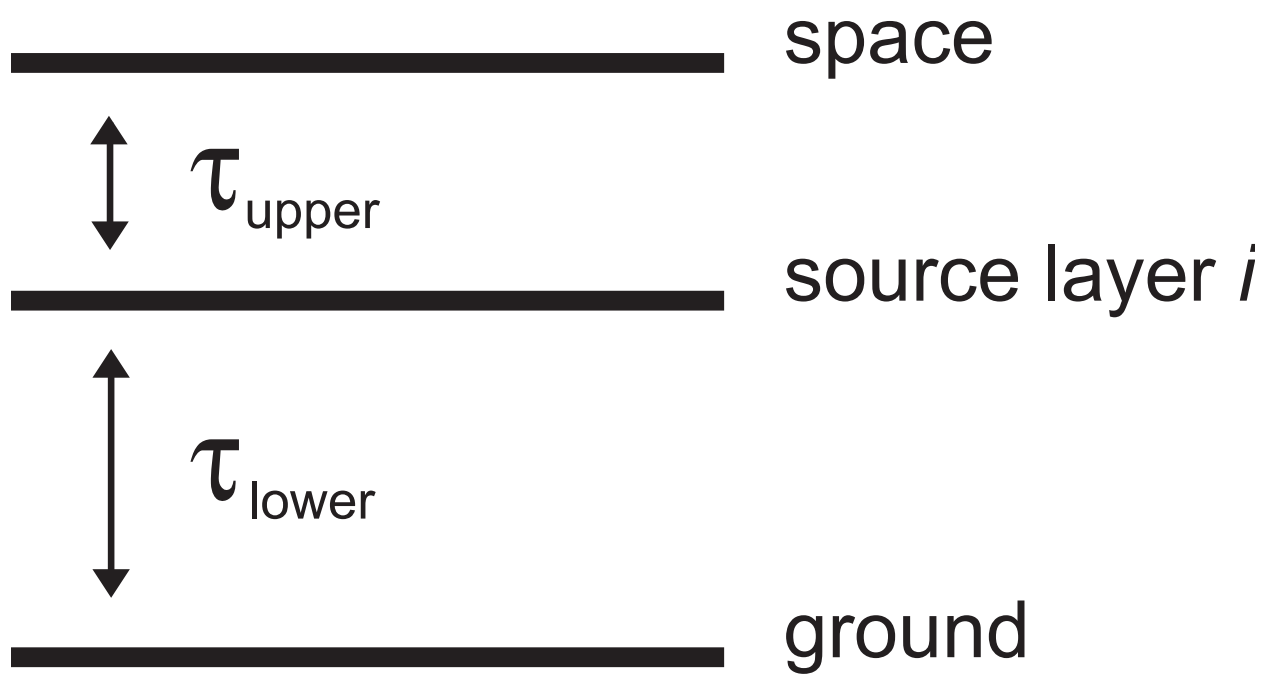


Fig. 15.— Diagram of the geometry of the UV redistribution layer and the surrounding atmosphere.